Extensive remineralization of peatland-derived dissolved organic carbon and acidification in the Sunda Shelf Sea, Southeast Asia

Yongli Zhou[1,*], Christopher D. Evans[2], Yuan Chen[1], Kristy Y.W. Chang[1, †], Patrick Martin[1,*]

[1] Asian School of the Environment, Nanyang Technological University, Singapore

[2] UK Centre for Ecology and Hydrology, Bangor, UK

[†] Current address: Singapore Centre for Environmental Life Sciences Engineering, Nanyang Technological University, Singapore

* Correspondence to zhou0303@e.ntu.edu.sg or pmartin@ntu.edu.sg

ORCID list

Yongli Zhou: 0000-0001-8403-6315

Christopher D. Evans: 0000-0002-7052-354X

Yuan Chen: 0000-0002-9625-0930

Kristy Y.W. Chang: 0000-0001-6387-2744

Patrick Martin: 0000-0001-8008-5558

Key words: terrigenous organic carbon, remineralization, acidification, Sunda Shelf Sea, tropical peatlands

Key Points:

- 60–70% of the dissolved organic carbon exported from the tropical peatlands is remineralized in the coastal waters of the Sunda Shelf
- This drives a seasonal acidification by 0.10 pH units and a net CO_2 efflux of 4.1–8.2 mol C m^{-2} yr^{-1} in the central Sunda Shelf
- 20–30% of the peatland-derived dissolved organic carbon might be relatively refractory and exported to the open Indian Ocean

Abstract

Southeast Asia is a hotspot of riverine export of terrigenous organic carbon to the ocean, accounting for ~10% of the global land-to-ocean riverine flux of terrigenous dissolved organic carbon (tDOC). While anthropogenic disturbance is thought to have increased the tDOC loss from peatlands in Southeast Asia, the fate of this tDOC in the marine environment and the potential impacts of its remineralization on coastal ecosystems remain poorly understood. We collected a multi-year biogeochemical time series in the central Sunda Shelf (Singapore Strait), where the seasonal reversal of ocean currents delivers water masses from the South China Sea first before (during Northeast Monsoon) and then after (during Southwest Monsoon) they have mixed with run-off from peatlands on Sumatra. The concentration and stable isotope composition of dissolved organic carbon, and colored dissolved organic matter spectra, reveal a large input of tDOC to our site during Southwest Monsoon. Using isotope mass balance calculations, we show that 60–70% of the original tDOC input is remineralized in the coastal waters of the Sunda Shelf, causing seasonal acidification by up to 0.10 pH units. The persistent CO_2 oversaturation drives a CO_2 efflux of 4.1 – 8.2 mol C m^{-2} yr^{-1} from the Singapore Strait, suggesting that a large proportion of the remineralized peatland tDOC is ultimately emitted to the atmosphere. However, incubation experiments show that the remaining 30–40% tDOC exhibits surprisingly low lability to microbial and photochemical degradation, suggesting that up to 20–30% of peatland tDOC might be relatively refractory and exported to the open ocean.

Plain Language Summary

Peatlands are large stores of organic carbon and are extensively distributed across coastal Sumatra and Borneo in Southeast Asia. These peatlands give rise to a large flux of dissolved organic carbon via rivers to the Sunda Shelf Sea, the marginal sea in Southeast Asia, and land conversion of peatlands has likely increased this flux. In the marine environment, organic carbon can be remineralized to CO_2 by sunlight and by microbial respiration, but the fate of peatland tDOC in coastal waters of Southeast Asia remains unclear. In this study, we analyzed water samples collected from the Sunda Shelf and found that 60–70% of the dissolved organic carbon from peatlands is decomposed to CO_2 in the coastal waters of the shelf sea. We further found that this resulted in a decrease in seawater pH by 0.10 units, and that a large proportion of the CO_2 is probably emitted to the atmosphere. This implies that the reported increase in tDOC export due to peatland disturbance may have had a significant effect on coastal biogeochemistry and downstream greenhouse gas emissions.

1 Introduction

Southeast Asia harbors the majority of the world's tropical peatlands, which are widely distributed in coastal areas of Sumatra and Borneo and store around 69 Pg C of terrestrial organic carbon (Dommain et al., 2014; Page et al., 2011). Consequently, Southeast Asia is also a hotspot of terrestrial organic carbon export to the ocean: the fluvial flux of terrigenous dissolved organic carbon (tDOC) to the Sunda Shelf Sea is ~21 Tg C yr^{-1}, which accounts for ~10% of the annual global land-to-ocean tDOC flux by world's rivers (Baum et al., 2007; Moore et al., 2011). In addition, most of this peatland area has been anthropogenically disturbed by deforestation and land conversion (Miettinen et al., 2016), which is thought to have increased the peatland tDOC export to the ocean by 32% over the past three decades (Moore et al., 2013; Yupi et al., 2016). This ongoing anthropogenic pressure on peatlands could therefore have impacts extending into the marine environment of Southeast Asia, especially on the sensitive ecosystems such as coral reefs, which critically hinge on the biogeochemical processing of the peatland-derived tDOC in the shelf sea.

Our understanding of the biogeochemical fate of tDOC in the global oceans is still limited, and in particular the degree to which ocean margins are efficient filters or conduits of tDOC between land and ocean remains debated. On the one hand, numerous studies have indicated that tDOC can be extensively and rapidly remineralized within ocean margins, as reported for the North Sea (Kitidis et al., 2019; Painter et al., 2018), the Louisiana Shelf (Fichot & Benner, 2014) and the Arctic Shelf (Alling et al., 2008; Humborg et al., 2017; Kaiser et al., 2017;

Letscher et al., 2011; Semiletov et al., 2016). Remineralization of tDOC fuels strong CO_2 emissions from coastal waters (Cai, 2011; Chen & Borges, 2009; Roobaert et al., 2019) and causes acidification in shelf seas (Semiletov et al., 2016). This is consistent with the canonical view that the DOC pool in the deep oceans only contains trace amounts of terrigenous DOC, as indicated by the low lignin concentrations (Meyers-Schulte & Hedges, 1986; Opsahl & Benner, 1997). On the other hand, some studies suggest that tDOC sometimes undergoes more limited remineralization within the ocean margins, and that a correspondingly larger proportion is delivered to the open oceans. For example, Medeiros et al. (2015) found that 50–76% of the tDOC exported by the Amazon River reaches the open Atlantic Ocean, likely due to the rapid transport of tDOC across the shelf. This might also be linked to the prior degradation history of tDOC before reaching the sea, as removal of the most labile fractions may result in the remaining tDOC having only limited degradability in some river systems (Chupakova et al., 2018; Shirokova et al., 2019; Stubbins et al., 2017). Recent molecular evidence shows that some fractions of tDOC are refractory and are exported to the open ocean (Cao et al., 2018; Medeiros et al., 2016), and carbon isotope data suggest that the terrestrial contribution to the oceanic DOC pool might be up to 30%, which is higher than previously believed (Follett et al., 2014; Zigah et al., 2017). It therefore remains unclear exactly how much tDOC is remineralized within ocean margins globally, with the extent of tDOC remineralization likely depending on factors such as the composition of the tDOC and the water circulation across the shelf, and varying substantially between different regions. However, most research has hitherto focused on mid- to high-latitude regions, and more research is therefore needed in tropical shelf seas

that are the recipients of some of the highest global rates of tDOC input.

The peatland-draining rivers in Southeast Asia are characterized by very high DOC concentrations (1000–5000 μmol L^{-1}) and high colored dissolved organic matter (CDOM, 50–200 m^{-1}) (Alkhatib et al., 2007; Martin et al., 2018; Moore et al., 2011; Rixen et al., 2008; Wit et al., 2015, 2018), which are among the highest values found in rivers globally (Meybeck, 1982). However, these peat-draining rivers only show moderate-to-low CO_2 efflux relative to their high DOC concentrations (Müller-Dum et al., 2019; Müller et al., 2015; Wit et al., 2015). In addition, field surveys have typically revealed conservative mixing of DOC across peatland-draining river estuaries (Alkhatib et al., 2007; Martin et al., 2018; Rixen et al., 2008; Wit et al., 2015; Zhou et al., 2019). This suggests that remineralization of tDOC within the rivers is limited, possibly due to lack of oxygen, low pH and short water residence times (Wit et al., 2015), which means that a large proportion of the peatland-derived tDOC is presumably exported to the coastal sea. Consistent with this prediction, Zhou et al., (2019) estimated from fluorescent dissolved organic matter data that 20–40% of the bulk DOC pool in coastal waters of northwestern Borneo (with salinity >30) is of terrestrial origin, due to the large input of peatland tDOC. It is possible that a large proportion of this tDOC is remineralized after it is exported to the coastal waters, as suggested by the high photo-lability of Southeast Asian peatland tDOC (Martin et al., 2018; Rixen et al., 2008) and the large CO_2 emissions reported for the coastal waters of eastern Sumatra (Wit et al., 2018). Given the large scale of the potential anthropogenic perturbation to the peatland tDOC flux, it is particularly important to better

130 constrain the biogeochemical fate of this tDOC and the associated impacts on the shelf sea
131 environment.
132
133 Here, we analyzed a multi-year time series of dissolved organic carbon, carbonate system
134 parameters, and carbon stable isotope composition using a mass balance approach to quantify
135 the remineralization of peatland-derived tDOC in the Sunda Shelf. The seasonal acidification
136 in the shelf sea and CO_2 emissions driven by the tDOC remineralization were further quantified.
137 Laboratory decomposition experiments were performed to investigate the degradability of
138 peatland-derived tDOC and estimate tDOC export to the open ocean.
139
140
141
142
143
144
145
146
147
148
149
150

2 Materials and methods

2.1 Study area

We collected biogeochemical time-series data at two sites in the Singapore Strait, Kusu Island (1.226°N, 103.860°E) and Hantu Island (1.227°N, 103.747°E). Both sites have coral reefs with >70 species of hard coral, and coral cover of around 40–50% (Bauman et al., 2017; Huang et al., 2009; Januchowski-Hartley et al., 2020). The Singapore Strait is located in the center of the Sunda Shelf Sea, and is close to the coastal peatlands on Sumatra (Fig. 1), with water depth mostly less than 40 m. The annual average circulation runs from the South China Sea into the Indian Ocean through the Java Sea and the Malacca Strait (Gordon et al., 2012). However, the monsoon system causes the main ocean currents to reverse direction seasonally (Fig. 1) (Mayer et al., 2018; Mayer & Pohlmann, 2014). During the Northeast Monsoon (November to February), water flows from the South China Sea westwards through the Singapore Strait and along the coast of Sumatra. During the Southwest Monsoon (May to September), the currents reverse and flow back eastwards through the Singapore Strait, carrying river discharge from the Sumatran peatlands (Mayer & Pohlmann, 2014; Siegel et al., 2019). Water in the Malacca and Singapore Straits is well mixed due to strong tidal currents (Mayer & Pohlmann, 2014). Because spatial variability between our two sampling sites was much smaller than the seasonal variability, we do not distinguish the data by site in this analysis.

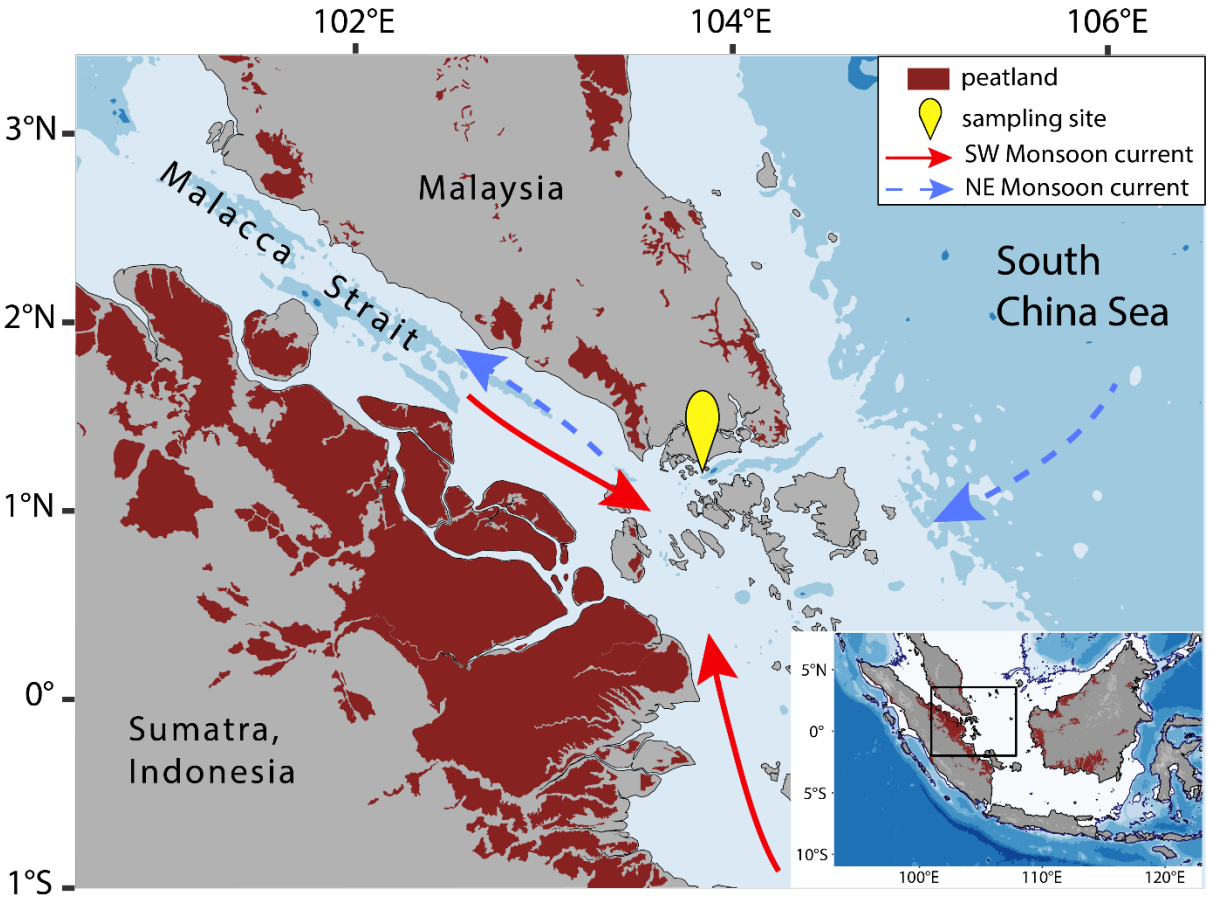

Figure 1. Map of the study region showing the location of tropical peatlands, the time series sampling site in the Singapore Strait and the directions of the prevailing ocean currents across the Sunda Shelf Sea. During the Northeast (NE) Monsoon season, the currents transport water from the open South China Sea to our study site; during the Southwest (SW) Monsoon season, the currents reverse and deliver water with inputs from the tropical peatlands along the east coast of Sumatra to our site, resulting in the seasonal variations in biogeochemistry.

2.2 Collection of water samples

Water samples were collected from both stations 1–2 times per month using a 1.5-L Niskin bottle at 5-m depth from October 2017 until August 2020. The water was immediately filtered on the boat through a pre-rinsed 47 mm diameter, 0.22 µm pore-size polyethersulfone membrane filter (Supor, Merck Millipore) in an in-line filter housing connected to a peristaltic pump and preserved for analyses of dissolved organic carbon (DOC), colored dissolved organic matter (CDOM) spectra, dissolved inorganic carbon (DIC), total alkalinity (TA), stable isotope

composition of DOC ($\delta^{13}C_{DOC}$) and of DIC ($\delta^{13}C_{DIC}$) (methods of collection are summarized in Table 1). The filter housing was bled of any air bubbles before collecting samples. Samples for chlorophyll-*a* were filtered onto 25 mm diameter Whatman GF/F filters instead, kept at −80°C and analyzed within 3 months of collection. At each station, a depth profile of salinity and temperature was measured by a fastCTD Profiler (Valeport Ltd).

Table 1. Collection and preservation of each biogeochemical parameter after filtration.

Parameter	Collection method	Preservation temperature
$\delta^{13}C_{DIC}$	1 ml of sample injected into a 12-ml Exetainer vial capped with butyl rubber septum containing 1 ml of ≥85% phosphoric acid and pre-flushed with helium.	20°C
DIC	A 12-ml Exetainer vial was filled to overflowing, left to overflow for 15s, and capped immediately with a butyl rubber septum to prevent gas exchange.	4°C
TA	Collected into a 140-ml HDPE bottle.	4°C
$\delta^{13}C_{DOC}$	Filled 40 ml into a 50-ml polypropylene centrifuge tube and stored frozen. Samples were thawed and acidified with 37% hydrochloric acid immediately prior to being sent off for analysis.	-20°C
CDOM	Filled 30 ml into a 40-ml pre-combusted EPA borosilicate vial.	4°C
DOC	Filled 30 ml into a 40-ml EPA borosilicate vial, acidified with 100 µl of 50% sulfuric acid.	4°C

2.3 Deployment of autonomous sensors

An SBE 19plus V2 SeaCAT CTD and a SeaFET pH sensor, equipped with copper biofouling

198 guards, (both Sea-Bird Electronics, Inc.) were deployed at Kusu Island in July 2015 to monitor
199 seawater salinity, temperature, and pH every 10 minutes. A SAMI-CO_2 sensor (Sunburst
200 Sensors), equipped with copper biofouling guards, was deployed at the same location from
201 March 2018 until July 2019 to measure the partial pressure of CO_2 (pCO_2) every two hours.
202 Sensors were attached horizontally to iron stakes hammered into the reef sediment at roughly
203 5 m depth along the reef slope and were retrieved every 1–3 months for data download and
204 maintenance.
205
206 The sensor data were validated with the CTD profile measurements and our measurements of
207 dissolved inorganic carbon and total alkalinity of water samples collected during each field
208 cruise, using the MATLAB CO2SYS Package Version 2.0 (referred to as CO2SYS below) (van
209 Heuven et al., 2011). The sensor data are presented as daily mean values. Data gaps occurred
210 whenever sensors were removed for maintenance or were sent for recalibration. The data
211 quality of the SAMI-CO_2 sensor was rapidly affected by biofouling and sediment accumulation
212 despite testing different sample pump and copper fouling guard configurations, and we
213 therefore stopped deploying it after July 2019.
214
215 **2.4 Sample analysis**
216 Dissolved inorganic carbon (DIC) was measured with an Apollo SciTech AS-C5 DIC analyzer
217 at room temperature (22±0.5°C) using an injection volume of 1 ml and a phosphoric acid
218 solution of 3% v/v phosphoric acid with 7% w/v sodium chloride. The phosphoric acid was

sparged with N_2 gas for 5 min prior to each analysis run. Each sample was measured 3–5 times to achieve a relative standard deviation of ≤0.1% for three replicate injections. Calibration was performed using the certified reference material (CRM) from Andrew Dickson's laboratory, Scripps Institution of Oceanography (Batch 172) or an in-house secondary standard made from Singapore Strait seawater that we calibrated against the CRM. The analytical precision for DIC was ±0.15% or lower based on replicate measurements of the CRM and the secondary standard.

Total alkalinity (TA) was measured with an Apollo SciTech AS-ALK2 titrator, which automates the Gran titration (Gran, 1952), using a ROSS combination glass pH electrode (Orion 8302BNUMD). Samples and standards were warmed to room temperature (22±0.5℃) and samples were measured 2–4 times in 25-ml aliquots using 0.1 M hydrochloric acid. The acid concentration was calibrated against the CRM or our in-house secondary standard. The analytical precision for TA was ±0.13% or lower based on replicate measurements of the CRM and the secondary standard.

Absorption spectra of CDOM were measured from 230 nm to 900 nm against a reference of ultrapure deionized water (18.2 MΩ cm^{-1}, referred to as DI water below) using a Thermo Evolution 300 dual-beam spectrophotometer in a 10-cm quartz cuvette. The absorption coefficients, the spectral slope $S_{275–295}$ (Helms et al., 2008), and the specific UV absorbance at 254 nm, $SUVA_{254}$ (Weishaar et al., 2003), were calculated using the "hyperSpec" package in R (Beleites & Sergo, 2012). We express the CDOM concentration as the absorption coefficient at

350 nm, a_{350}.

DOC samples (30 ml) were acidified with 100 µl of 50% sulfuric acid and analyzed on a Shimadzu TOC-L system with a high-salt combustion kit, using an injection volume of 150 µl and a 5-minute sparge time. Each sample was measured 5–7 times to achieve a coefficient of variation of ≤2%. Potassium hydrogen phthalate was used for calibration, and the analytical accuracy was monitored using certified deep-sea water reference material (42–45 µmol L^{-1} DOC) from the University of Miami, USA. Our analyses consistently yielded slightly higher values for the CRM, with a long-term mean and standard deviation of 48.0±3.9 µmol L^{-1} DOC.

The $\delta^{13}C_{DOC}$ samples were thawed, acidified to pH of 2–3 with 37% w/v hydrochloric acid, and shipped to the Ján Veizer Stable Isotope Laboratory, University of Ottawa, Canada for analysis using an OI Analytical Aurora Model 1030W TOC Analyzer interfaced to a Finnigan Mat DeltaPlusXP isotope ratio mass spectrometer. The 2-sigma analytical precision is ±0.4‰ (https://isotope.uottawa.ca/en/services-waters).

$\delta^{13}C$ of DIC measurements were made using a Gas Bench connected to an isotope ratio mass spectrometer at the Stable Isotope Facility, University of California, Davis (UC Davis) and by ourselves at the Marine Geochemistry Laboratory, Nanyang Technological University, Singapore (NTU). At NTU, final $\delta^{13}C$ values were obtained after instrumental drift correction, blank correction for standards (Assayag et al., 2006; Humphreys et al., 2016), and calibration

using NBS-18 ($\delta^{13}C = -5.01‰$) and Estremoz ($\delta^{13}C = 1.63‰$) calcium carbonate standards. All $\delta^{13}C$ values of the samples were further corrected by accounting for the difference between the international consensus value of $\delta^{13}C_{DIC}$ of the Dickson CRM (0.78‰) (Cheng et al., 2019) and our laboratory measurements of $\delta^{13}C_{DIC}$ of the Dickson CRM at NTU (the magnitude of this correction was mostly below 0.4‰). The long-term standard deviation for $\delta^{13}C$ of DIC measurements at UC Davis is reported as ±0.1‰ (https://stableisotopefacility.ucdavis.edu/) and at NTU was ±0.2‰ (Carrara marble, n=24, 4 runs).

Chlorophyll-*a* was extracted in 90% acetone at 4°C in the dark for 24 hours and measured on a HORIBA Floromax-4 fluorometer with excitation at 436 nm and emission at 680 nm, with bandpasses of 5 nm (Welschmeyer, 1994). Data were normalized to the reference signal and calibrated using a spinach chlorophyll-*a* standard (Sigma-Aldrich C5753).

2.5 Analyses of the time-series data

Due to the monsoonal current reversal, the Singapore Strait seasonally receives water directly from the South China Sea with little terrestrial influence. This water subsequently mixes with peat-draining river input off the coast of Sumatra, and then seasonally flows back into the Singapore Strait when the currents reverse direction (Fig. 1). The seasonal variation in the Singapore Strait is therefore equivalent to the spatial variability from the South China Sea into the coastal waters of Sumatra in the Malacca and Karimata Straits, and therefore reflects the mixing of water from the open sea with peatland-draining river input.

Our data analysis consists of two components: first, we built a conservative mixing model to predict the values of DIC, TA, pH and $\delta^{13}C_{DIC}$ if this mixing was strictly conservative. We therefore interpret any deviations in our measurements relative to the predicted values as indicative of biogeochemical processing. Second, we performed isotope mass balance calculations for DOC and the carbonate system to estimate how much of the DOC pool was tDOC, how much of the excess DIC (relative to conservative mixing) was contributed from tDOC remineralization, and, when the measured deviations in $\delta^{13}C_{DIC}$ were greater than could be explained from the measured deviation in DIC concentration, how much additional tDOC must have been remineralized and already outgassed upstream of our site to explain the measured $\delta^{13}C_{DIC}$. These calculations are summarized in Fig. 2 and below, and full details are provided in the Supplementary Information.

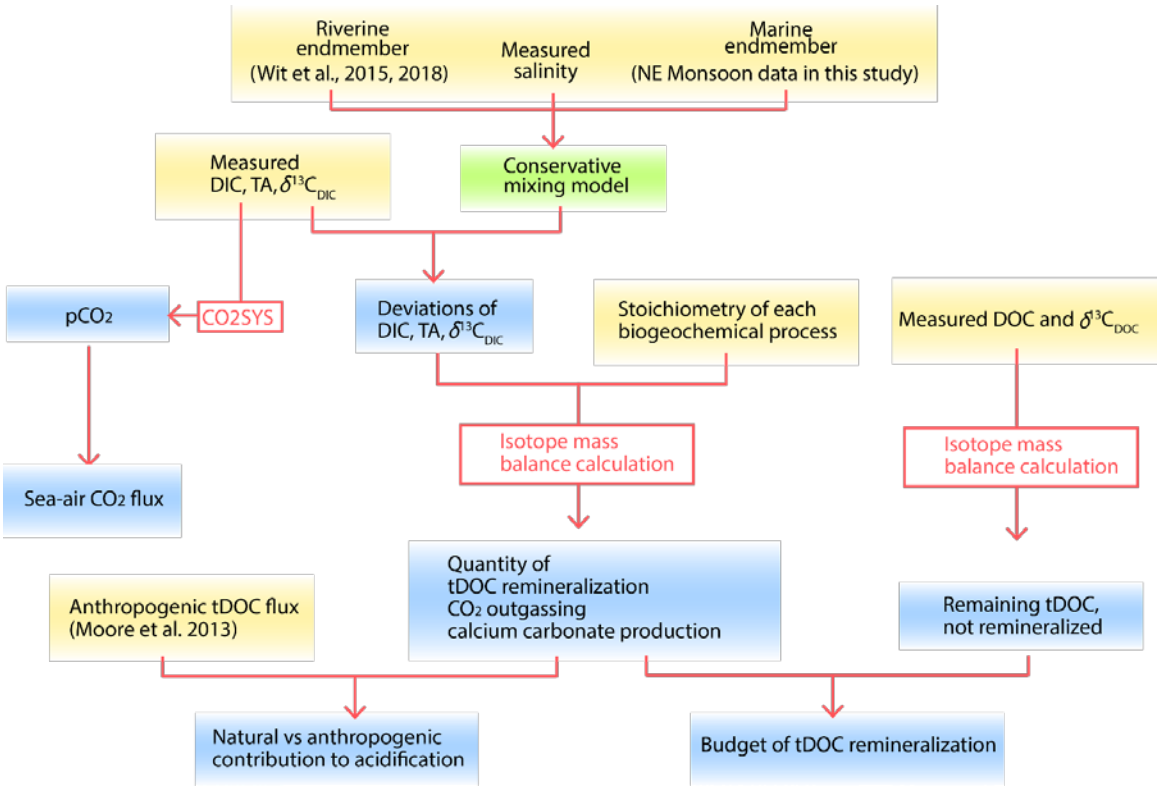

Figure 2. A flowchart summarizing the data analyses for this study. Yellow boxes indicate the inputs and blue boxes indicate outputs of calculations. We built a conservative mixing model to predict the biogeochemical parameters if there was only mixing between riverine water and marine water. Isotope mass balance calculations were performed with the deviations of the measured data from the mixing model to quantify tDOC remineralization and the potential anthropogenic contribution to the seasonal acidification.

2.5.1 Conservative mixing model

We built a two-endmember mixing model to calculate the DIC, TA, pH and $\delta^{13}C_{DIC}$ expected from conservative mixing between the riverine endmember and the marine endmember. This allowed us to calculate the deviations of the measured data from the values expected from conservative mixing. The relative contribution of riverine input and marine input was calculated from the measured salinity. Seawater pH expected from conservative mixing was calculated from the DIC and TA of conservative mixing by CO2SYS.

We calculated the discharge-weighted average of the published data of DIC, TA (calculated

313 from pH and pCO_2) and $\delta^{13}C_{DIC}$ from the main peat-draining rivers on Sumatra (the Batanghari,
314 Indragiri, Kampar and Siak Rivers) (Wit et al., 2015, 2018), which we adopted as the riverine
315 endmember values. The marine endmember values were estimated from our measurements in
316 the Singapore Strait from the end of the NE Monsoon and the subsequent inter-monsoon season
317 (late February to March), when the water in the Singapore Strait consists predominantly of
318 marine water from the open South China Sea and our data indicated minimal presence of tDOC
319 and freshwater input (Section 3.1). All the endmember values and the uncertainties are provided
320 in Table 2.
321
322
323 **2.5.2 Isotope mass balance calculations**
324 Based on the known changes in DIC, TA and $\delta^{13}C_{DIC}$ relative to the values expected from
325 conservative mixing caused by primary production, remineralization, calcium carbonate
326 production and dissolution and air-sea CO_2 exchange (Zeebe & Wolf-Gladrow, 2001) (Table
327 S1), we back-calculated the amount of carbon that had been processed by these biogeochemical
328 processes from the measured deviations in DIC, TA and $\delta^{13}C_{DIC}$ using an isotope mass balance
329 approach following Samanta et al. (2015). The proportion of the bulk DOC pool that was tDOC
330 was calculated from the measured $\delta^{13}C_{DOC}$ and DOC concentration.
331
332 The $\delta^{13}C_{DOC}$ data were not available for rivers on Sumatra, but the $\delta^{13}C_{DOC}$ values of the
333 peatland-derived tDOC across peatlands on Sumatra and rivers on Borneo and Peninsular

334 Malaysia mostly range between −30‰ and −28‰ (Baum, 2008; Evans et al., 2014; Gandois
335 et al., 2014; Zhu et al., 2020). We therefore adopted −29‰ as the riverine endmember value
336 of $\delta^{13}C_{DOC}$ for the peatland-derived tDOC. For the $\delta^{13}C$ of the DIC produced from
337 remineralization, microbial respiration causes little carbon isotopic fractionation, while results
338 from our experiments (Section 3.6) and previous studies (Opsahl & Zepp, 2001; Osburn et al.,
339 2001; Spencer et al., 2009) indicated that photodegradation (and combined photo-bio-
340 degradation) of tDOC can cause fractionation in $\delta^{13}C$ of −1.4‰ to −5.8‰ between the
341 produced DIC and the initial DOC (Table S2). Because of the low bio-degradability (Nichols
342 & Martin, submitted) but high photo-degradability of Southeast Asian peatland tDOC (Section
343 3.6), we infer that a major part of the remineralization of tDOC in this region might be via
344 photodegradation, and therefore entails a carbon isotopic fractionation. We adopted a
345 fractionation of −3‰, and thus used −32‰ as the $\delta^{13}C$ of the DIC produced from tDOC
346 remineralization. Note that by assuming this additional fractionation, our calculated amount of
347 remineralized tDOC is smaller, since a smaller amount of carbon is needed to yield the
348 observed $\delta^{13}C_{DIC}$ values.
349
350 These mass balance calculations provide the quantity of (i) the amount of tDOC at our site,
351 representing the remaining fraction of the tDOC input from peatlands that has not been
352 remineralized, (ii) the remineralized tDOC as DIC, (iii) the remineralized tDOC that had been
353 removed by outgassing from the DIC pool upstream of our sampling site, and (iv) the amount
354 of calcium carbonate production and dissolution. The sum of the fractions (i) – (ii) represents

355 the initial concentration of tDOC for a given salinity after estuarine mixing and before
356 biogeochemical processing has occurred.
357
358 The uncertainty of the mass balance calculations was estimated by a Monte Carlo algorithm,
359 in which we perturbed each input parameter with a 1σ normally distributed error (Table 2) by
360 random sampling, repeated the calculations 10,000 times, and then calculated the resulting
361 standard deviation of each output parameter. For the riverine endmember values as input
362 parameters, the 1σ error of the DIC and TA were adopted from Wit et al. (2018); the 1σ error
363 of the $\delta^{13}C_{DIC}$ and $\delta^{13}C_{DOC}$ were both assumed to be ±1‰, because the uncertainties are not
364 available and the reported $\delta^{13}C_{DOC}$ values of the peatland-derived tDOC in Southeast Asia
365 mostly range between −30‰ and −28‰. The 1σ error of the marine endmember variables
366 are the standard deviations of the measurements from late February to March. The 1σ error of
367 the measured DOC, DIC, TA, $\delta^{13}C_{DIC}$ and $\delta^{13}C_{DOC}$ are the long-term 1σ precision of
368 measurements of the standard materials. The 1σ error of the measured salinity (±0.01) was
369 estimated based on the accuracy of the conductivity measurement of the Valeport fastCTD
370 (±0.01 mS cm^{-1}).
371
372 **2.5.3 Acidification and putative anthropogenic contribution**
373 Seasonal acidification was indicated by the time series measurements of DIC and TA and the
374 SeaFET pH sensor data (Section 3.5). Saturation states of calcite and aragonite were calculated
375 from the DIC and TA data by CO2SYS.

From the results of the mass balance calculations, we further reconstructed the individual contribution to the deviations of DIC and TA from (i) calcium carbonate dissolution, (ii) remineralization of natural tDOC, and (iii) remineralization of anthropogenic tDOC. The reconstructed DIC and TA deviations were translated to the pH deviations relative to conservative mixing by CO2SYS for assessment of the putative anthropogenic contribution to the observed acidification. We distinguished the natural tDOC remineralization from the anthropogenic component based on the report that 35% of the tDOC flux is caused by peatland perturbations (Moore et al., 2013). While this estimate is based on a limited and small-scale comparison of disturbed and intact peatland catchments that has yet to be demonstrated at large scales, it has already been applied by several other studies to gain insight into the possible downstream impacts of peatland disturbance (Wit et al., 2018).

2.5.4 Sea-air CO_2 flux

We calculated the annual areal sea-air CO_2 flux following Lønborg et al. (2019) using the pCO_2 calculated from the measured DIC and TA (the *in-situ* sensor record was too limited to be used). We obtained average wind speeds for the area of 0.5°N–1.5°N and 102.5°E – 105.5°E from the CYGNSS Level 2 Science Data Record Version 2.1 (CYGNSS, 2017). The gas transfer velocity was calculated following Wanninkhof et al. (2009). The CO_2 solubility was calculated following Weiss (1974) using the measured water temperature. The uncertainty of the CO_2 flux was estimated by a Monte Carlo algorithm, based on the uncertainty of the salinity, DIC and

397 TA measurements (Table 2) and the reported uncertainty of the wind speed measured by
398 CYGNSS (±1.4 m/s) (Ruf et al., 2019).
399
400 **2.6 Degradation experiments**
401 Incubation experiments were performed to determine the degradability of tDOC by photo-
402 chemical remineralization and by microbial remineralization. For photo-chemical
403 remineralization, we additionally measured the carbon isotopic fractionation.
404
405 For photodegradation experiments, surface water samples (<1m depth) were collected from the
406 Maludam River in Malaysia (1.636°N 111.049°E), which drains a large area of intact peatland
407 on northwestern Borneo, in December 2018 and June 2019, and from Kusu Island in the
408 Singapore Strait in January 2020 (NE Monsoon) and July 2020 (SW Monsoon). Samples were
409 filtered through pre-rinsed Whatman Polycap filters or 0.22 µm pore-size polyethersulfone
410 membrane filters on the day of collection, stored at 4°C and re-filtered prior to the experiments.
411 For the filtered water collected from the Maludam River in December 2018 and from the
412 Singapore Strait, we filled 40 ml aliquots into replicate cylindrical quartz cells (50 mm
413 pathlength, 50 mm diameter, with Teflon screw caps) and irradiated the samples in an Atlas
414 Suntest CPS+ solar simulator fitted with a xenon lamp and daylight optical filter. The
415 temperature control was set to 40 °C (the lowest possible setting), and light output between
416 300–400 nm was set to 40 W m^{-2}. The quartz cells were opened and ventilated regularly to
417 avoid depletion of oxygen and then recapped. A dark control was prepared by filling 200 ml

418 filtered water into a 250 ml Duran glass bottle, which was wrapped in aluminum foil and placed
419 in the solar simulator. One or two replicate quartz cells were removed at regular time-points to
420 measure DOC and CDOM (using 2-mm, 1-cm, or 10-cm pathlength quartz cuvettes) with
421 parallel measurements of the dark control.
422
423 To measure carbon isotopic fractionation associated with photodegradation, the filtered water
424 collected from the Maludam River in June 2019 was filled into replicate 150-ml quartz bottles
425 with ground stoppers, leaving 30 ml headspace, and placed in an unshaded outdoor location at
426 Nanyang Technological University, Singapore. Weather conditions during the experiment were
427 partly sunny on most days, sometimes with heavy rain showers lasting up to a few hours. The
428 ambient temperature varied between 26–32°C within a diurnal cycle. The quartz bottles were
429 opened and ventilated once a week to avoid oxygen depletion and then recapped. A dark control
430 was prepared as above, and placed in the same location. One replicate bottle was removed to
431 measure DOC, CDOM (using 2-mm or 1-cm pathlength quartz cuvettes) and $\delta^{13}C_{DOC}$ on Days
432 0, 60 and 98, with parallel measurements of the dark control.
433
434 For the biodegradation experiment, 10 L of surface water (<1m depth) was collected from Kusu
435 Island in the Singapore Strait in July 2020 (SW Monsoon), part of which was kept unfiltered
436 as an inoculum while the rest was filtered through 0.22 μm pore-size polyethersulfone
437 membrane filters one day after collection. Three treatments were created: filtered water only
438 (as sterile control), filtered water + inoculum (v/v = 5%), and filtered water + inoculum + labile

DOC (leucine and glucose, each contributed approximately 10 μmol L^{-1} carbon, to test for a possible priming effect). For each treatment, replicate 150 ml aliquots of the appropriate water sample were filled into 250-mL Duran glass bottles, capped with airtight Teflon screw caps, and kept in the dark in a shaded outdoor location at Nanyang Technological University, Singapore. The ambient temperature varied between 26–32°C within a diurnal cycle. Bottles were gently swirled every other day. For each treatment, three replicate samples were removed and filtered through 0.22 μm pore-size polyethersulfone membrane filters for DOC and CDOM measurements on Days 0, 3, 7, 14, 27, 48 and 109. Bottles were cleaned with 10% hydrochloric acid and DI water and combusted at 450 ℃ for 4 hours before use.

460 **3 Results**

461 **3.1 Monsoon-driven seasonal variation of tDOC input to the Singapore Strait**

462 During the SW Monsoon, the currents transport water from the east coast of Sumatra and the
463 Malacca Strait to our sampling site in the Singapore Strait. These waters receive large riverine
464 inputs from the extensive peatlands on Sumatra, and correspondingly we observed a decrease
465 in salinity from ~33 to ≤30 during this period (Fig. 3a, Fig. S1a). The DOC concentration
466 increased to 75–100 μmol L^{-1}, which was 10–35 μmol L^{-1} higher than in the inter-monsoon
467 seasons (Fig. 3c). The CDOM absorption (a_{350}) increased to 0.5–2 m^{-1}, which was 2–10 times
468 higher compared to inter-monsoon seasons (Fig. 3d). In addition, the SW Monsoon exhibited
469 the lowest spectral slope of CDOM ($S_{275\text{-}295}$) (0.016–0.020 nm^{-1}), the highest $SUVA_{254}$ (2–3 L
470 mg^{-1} m^{-1}) and the lightest $\delta^{13}C_{DOC}$ (−25.5 to −24‰) of the year, all of which indicate a large
471 input of tDOC (Fig. 3e–g). The mass balance calculations showed that 20–50% of the DOC
472 pool in the Singapore Strait was terrigenous during this period (Fig. 3h).

473

474 During the early NE Monsoon (Dec–Jan), when the water flows from the South China Sea, we
475 also observed a brief decrease in salinity by ~2 units. Because this is the time of year with the
476 greatest precipitation in Singapore and southern Malaysia, some freshwater input from run-off
477 would be expected at this time. However, the DOC and CDOM concentrations, the $SUVA_{254}$,
478 the $S_{275\text{-}295}$, and the $\delta^{13}C_{DOC}$ only showed small changes relative to the inter-monsoon periods
479 (Fig. 3c–g), which suggest that the tDOC input was limited. During the late NE Monsoon and
480 the following inter-monsoon season (late February to March; the season with lowest local

481 precipitation), continued water flow from the open South China Sea results in the highest
482 salinity of the year (~32–33), low DOC concentration (~65 μmol L^{-1}), low a_{350} (<0.25 m^{-1}),
483 high $S_{275\text{-}295}$ (>0.026 nm^{-1}) and more enriched values of $\delta^{13}C_{DOC}$ (−23 to −21‰) (Fig. 3c–g).
484 We therefore took the averages of our data during this period as the marine endmember values
485 for the conservative mixing model (Table 2).
486
487 The seawater temperature showed only small seasonal variation, mostly between 28–31°C (Fig.
488 3b). The chlorophyll-*a* concentration mostly ranged between 0.5–2 μg L^{-1} and showed no clear
489 seasonal variation (full data set in Supplementary Data Table).
490

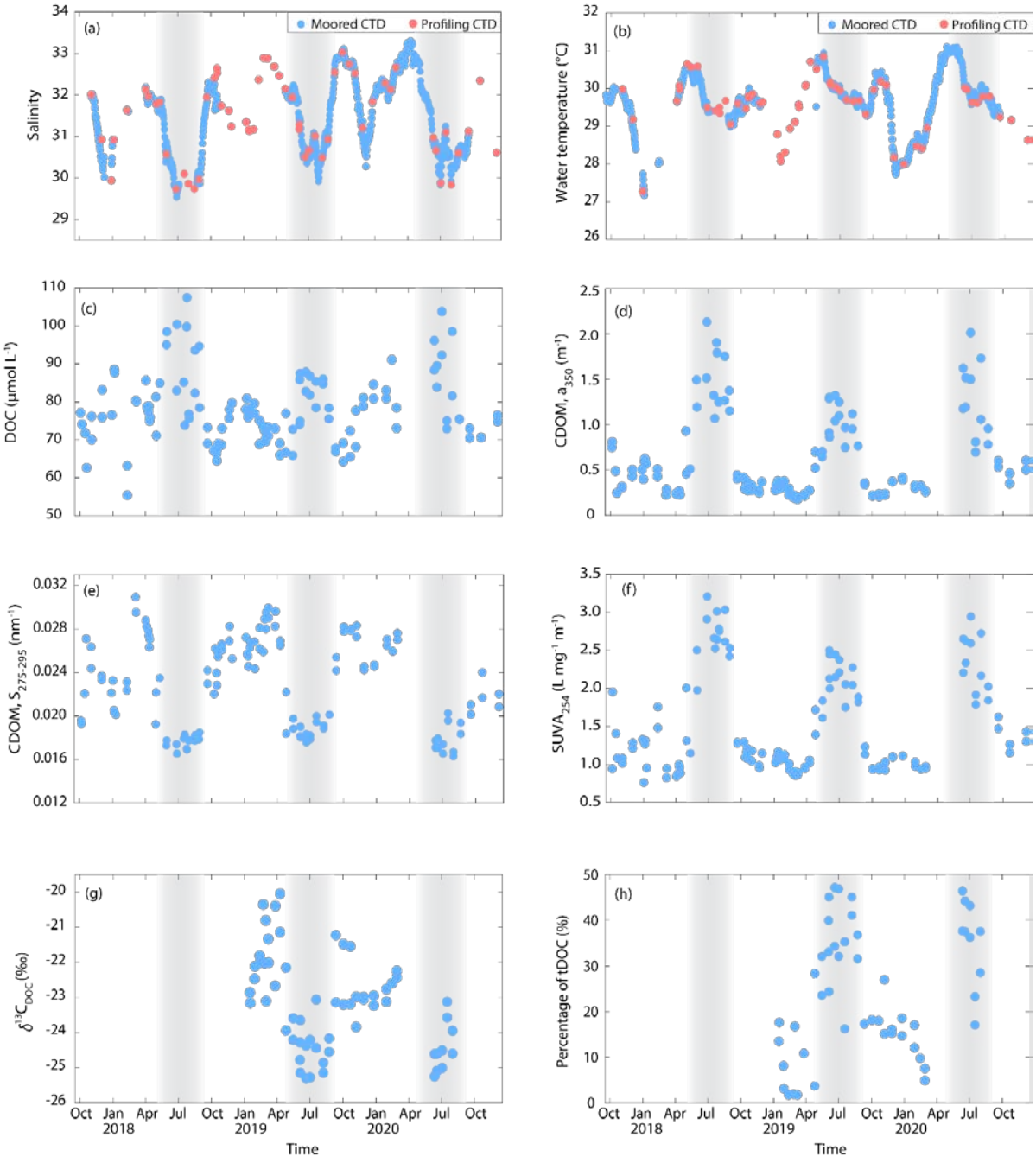

Figure 3. Seasonal variations in biogeochemistry in the Singapore Strait. Time series of **(a)** salinity, **(c)** DOC, **(d–f)** CDOM and **(g)** stable isotopic composition ($\delta^{13}C$) of DOC indicates a large input of freshwater and terrigenous dissolved organic matter to our site during the Southwest Monsoon season (May to September, highlighted by grey shading). The water temperature **(b)** shows small seasonal variation by ~3°C. The salinity and water temperature were both measured by a profiling CTD during each sampling cruise and by a moored CTD. The percentage of tDOC in the bulk DOC pool **(h)** was estimated from the $\delta^{13}C_{DOC}$ data.

Table 2. Endmember values (± 1SD) and the uncertainties (shown as ± 1SD) of the parameters measured at our site as input to the conservative mixing model and Monte Carlo uncertainty calculation.

Parameter	Riverine endmember	Marine endmember	Uncertainty of measured data
Salinity	0	32.69 ± 0.23	± 0.01
DIC (μmol kg^{-1})	453 ± 34	1903 ± 13	± 0.15%
TA (μmol kg^{-1})	310 ± 34	2164 ± 15	± 0.13%
$\delta^{13}C_{DIC}$ (‰)	-15.32 ± 1	-0.25 ± 0.09	± 0.2
$\delta^{13}C_{DOC}$ (‰)	-29 ± 1	-21.88 ± 0.79	± 0.2
$\delta^{13}C_{tDIC}$ (‰)*	-32 ± 1	-	-
DOC (μmol L^{-1})**	-	-	± 3.9

* The $\delta^{13}C$ of DIC produced from remineralization of peatland-derived tDOC.

** DOC endmember values were not used in the calculations.

3.2 Seasonal variation of DIC, TA and $\delta^{13}C_{DIC}$ driven by tDOC remineralization

During the SW Monsoon, the DIC was mostly 15–40 μmol kg^{-1} higher than the values expected from the conservative mixing model, while the TA typically showed a depletion of 10–40 μmol kg^{-1} relative to conservative mixing (Fig. 4a, b). By comparing the measured deviations with the known changes caused by different biogeochemical processes, we found that the variation in DIC and TA during the SW Monsoon was chiefly the result of remineralization and calcium carbonate production (Fig. 4c). Because the Singapore Strait was always oversaturated with respect to pCO_2 (Section 3.4), net CO_2 outgassing, instead of CO_2 invasion, is expected throughout the year. Because the net CO_2 outgassing and calcium carbonate production both remove DIC from seawater, it is likely that the total quantity of remineralized tDOC is in fact greater than the measured positive deviation of DIC concentration during the SW Monsoon. We therefore turn to $\delta^{13}C_{DIC}$ to estimate the total amount of tDOC remineralization.

520 The $\delta^{13}C_{DIC}$ in the inter-monsoon seasons varied between -0.4 and 0‰. It decreased to
521 between -1.0 and -1.8‰ during the SW Monsoon (Fig. 4d). However, our conservative
522 mixing model predicts that $\delta^{13}C_{DIC}$ would vary by only 0.3‰ as a result of riverine DIC input
523 (Fig. 4d). This small predicted range is a result of the low DIC concentration in peat-draining,
524 low-pH rivers. The remaining 0.7–1.5‰ decrease in the $\delta^{13}C_{DIC}$ therefore indicates production
525 of extra DIC from an isotopically depleted carbon source, consistent with the remineralization
526 of tDOC within the shelf waters.
527
528

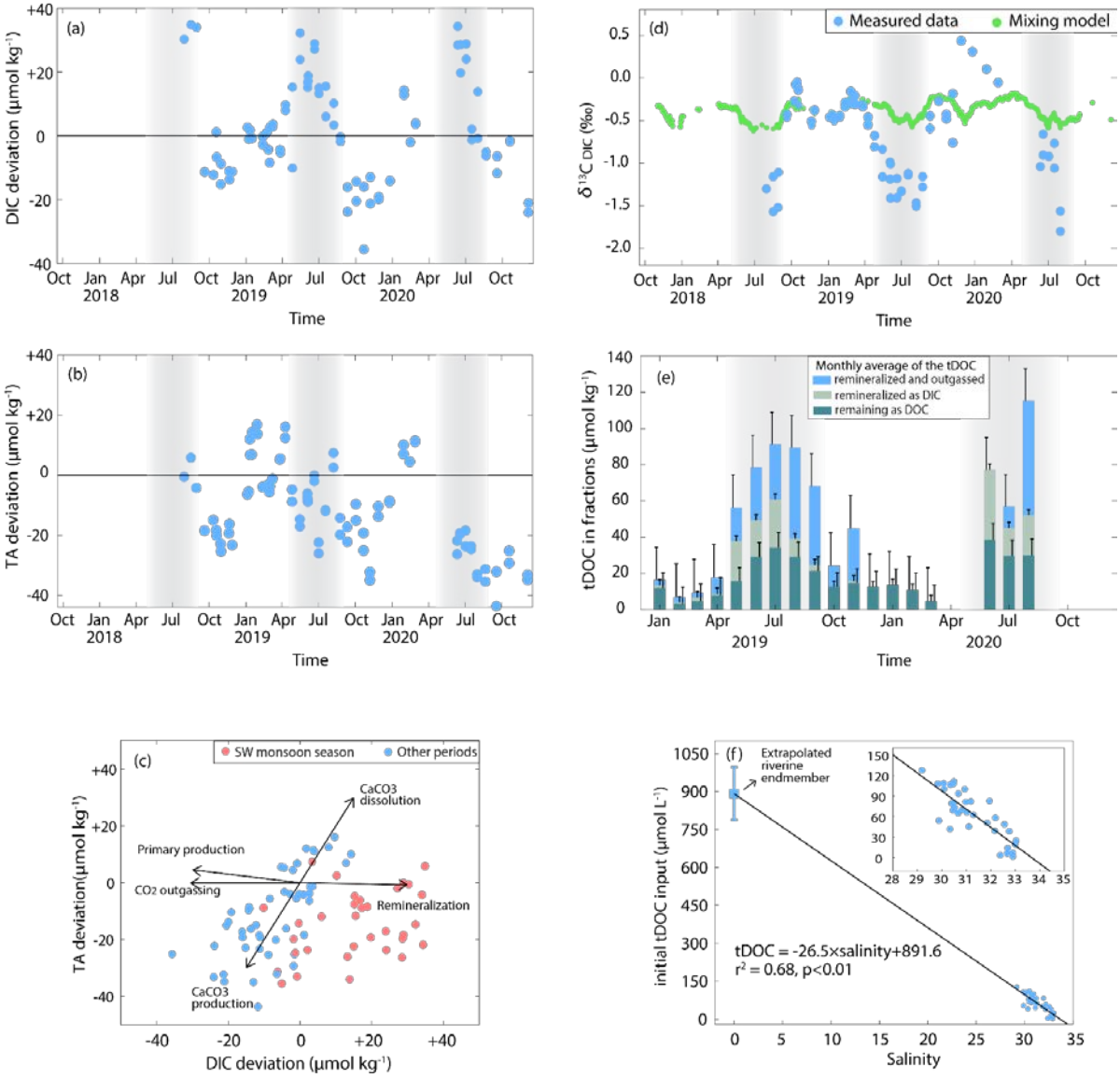

Figure 4. (a – b) Time series of deviations of DIC and TA relative to values expected from the conservative mixing model. DIC shows positive deviation during the SW Monsoon Season (grey shading), coincident with the large tDOC input. **(c)** Scatterplot of deviation of DIC versus deviation of TA, which indicates a strong signal of remineralization during the SW Monsoon season. **(d)** The $\delta^{13}C$ of DIC showed strong depletion relative to the mixing model during the SW Monsoon season, indicating remineralization of tDOC. **(e)** Monthly average quantity of (1) the remaining tDOC, (2) remineralized tDOC that was still present as DIC, (3) remineralized tDOC that had already outgassed to the atmosphere; as estimated by the isotope mass balance calculations. The total height of each stacked bar represents the total initial tDOC concentration in that water before remineralization. The error bars show one standard deviation of each tDOC fraction, as estimated by a Monte Carlo simulation (shown in one direction for clarity). **(f)** The relationship between salinity and the total initial tDOC concentration yields a predicted peatland riverine endmember DOC concentration of 892±104 µmol L^{-1} (mean ± standard error).

3.3 Quantification of tDOC remineralization by isotope mass balance calculations

The isotope mass balance calculations provide a breakdown of tDOC remineralization into three fractions (see Section 2.4.2). We assumed that all remineralized terrigenous carbon is derived from tDOC, i.e. that terrigenous POC does not contribute to the signals we observe, and that production and remineralization of autochthonous (i.e., marine) DOC are approximately in steady state and do not vary seasonally. The validity of these assumptions is discussed in Section 4.1.

Our SW Monsoon data (Fig. 4e) show that the initial total tDOC concentration (represented by the total height of each stacked bar) amounted to between 60–140 μmol kg^{-1}. Of this initial tDOC, 20–40 μmol kg^{-1}, or 30–40%, was still present as unremineralized tDOC at our site, while the remaining 60–70% had been remineralized in the shelf sea before reaching our site. Of this remineralized tDOC, 10–40 μmol kg^{-1} was still present in the DIC pool, while 15–80 μmol kg^{-1} had been lost to the atmosphere. The proportion of remineralized tDOC that had been removed by outgassing increased over the course of the SW Monsoon. The uncertainty of each carbon fraction ranged from 5–15 μmol kg^{-1} as estimated by a Monte Carlo simulation, indicating an overall quite well-constrained tDOC budget.

The initial total tDOC concentration showed a strong linear relationship with salinity ($[DOC] = -26.5 \times salinity + 891.6$, r^2=0.68, p<0.01, Fig. 4f), the intercept of which implies an average riverine endmember DOC concentration of 892 ± 104 μmol L^{-1} (mean ± standard error). This

565 value is in remarkably close agreement with the reported discharge-weighted mean DOC
566 concentration of Sumatra's main peat-draining rivers, which is 890 ± 159 μmol L^{-1} (Wit et al.,
567 2015), and is too high to be explained by non-peatland tDOC sources.
568
569 **3.4 Seasonal variation of pCO_2 and the sea-air CO_2 yield**
570 The pCO_2 in the Singapore Strait showed oversaturation throughout the year, as well as
571 pronounced seasonal variation. During the inter-monsoon season, pCO_2 was below 500 μatm,
572 but it increased to 550–700 μatm during the SW Monsoon (Fig. 5a), consistent with
573 remineralization of tDOC having occurred prior to reaching the Singapore Strait. The high
574 pCO_2 values during the SW Monsoon translated to a daily areal sea-to-air CO_2 flux of 15–68
575 mmol C day^{-1} m^{-2} (Fig. 5b). The annual areal sea-to-air CO_2 flux in the Singapore Strait,
576 amounted to 4.10±0.47 mol C m^{-2} yr^{-1} in 2019 and 8.20±1.17 mol C m^{-2} yr^{-1} in 2020.
577

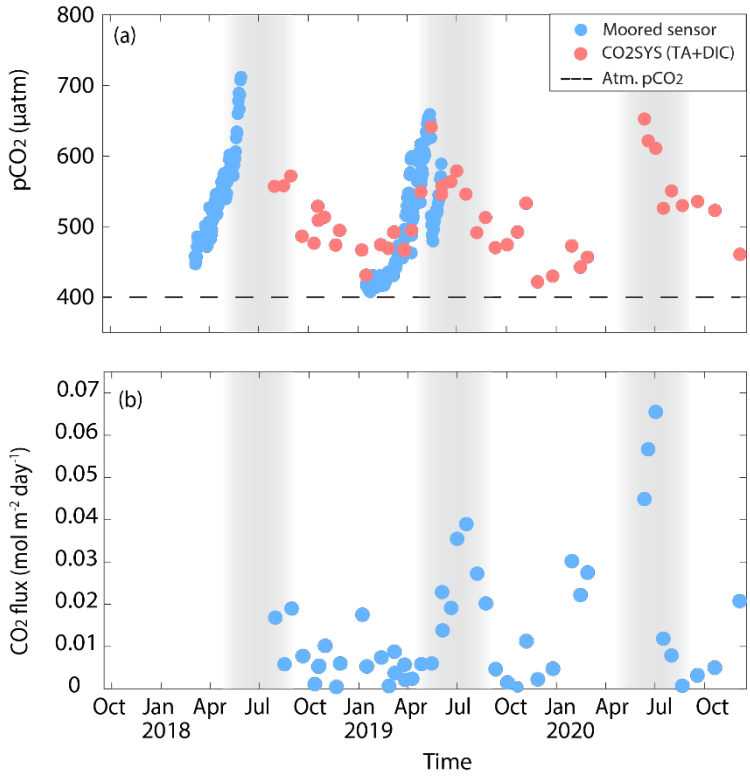

Figure 5. Time series of **(a)** pCO_2 and the **(b)** daily areal CO_2 flux. The pCO_2 was measured by a moored SAMI pCO_2 sensor and was validated by the laboratory analysis of TA and DIC using CO2SYS. The data from the latter approach were used for calculation of the CO_2 yield. The Southwest Monsoon season is highlighted by the grey shading.

3.5 Seasonal acidification and putative anthropogenic contribution

Seawater pH in the Singapore Strait was 7.95–8.03 during the NE Monsoon and the inter-monsoon seasons, when terrestrial input was minor. The pH decreased by up to 0.14 units, to 7.90–7.85, during the SW Monsoon (Fig. 6a, Fig. S1b). This pH decrease could be driven by freshwater input, calcium carbonate production, and/or remineralization of organic carbon. Our conservative mixing model only predicts decreases in seawater pH at our site of ~0.02 units, indicating that input of river water can only explain a small proportion of this variation (Fig. 6a). The contribution from calcium carbonate production was constrained from the isotope

593 mass balance calculations, and was only responsible for a small additional pH reduction, mostly
594 <0.02 units (Fig. 6b). The majority of the pH decrease, 0.06–0.10 units, was therefore
595 attributable to the remineralization of tDOC. Assuming that 35% of the total tDOC input during
596 the SW Monsoon, and hence also 35% of the tDOC remineralization, might be an
597 anthropogenic contribution caused by peatland disturbance (Moore et al., 2013; Yupi et al.,
598 2016), we further estimate that 0.01–0.04 pH units of this seasonal acidification could be
599 anthropogenic (Fig. 6b).
600
601 This seasonal variation in the carbonate system also entails changes in the saturation state of
602 calcite (Ω_{CA}) and aragonite (Ω_{AR}). During the late NE Monsoon and inter-monsoon, Ω_{CA} and
603 Ω_{AR} were 4.62±0.09 and 3.07±0.06, respectively (Fig. 6c). During the SW Monsoon, the Ω_{CA}
604 decreased to 3.2–4.0 and the Ω_{AR} decreased to 2.1–2.7. These decreases exceeded the decreases
605 predicted by the conservative mixing model by a factor of ≥2, demonstrating the potential for
606 tDOC remineralization to affect calcifying communities in this region.
607

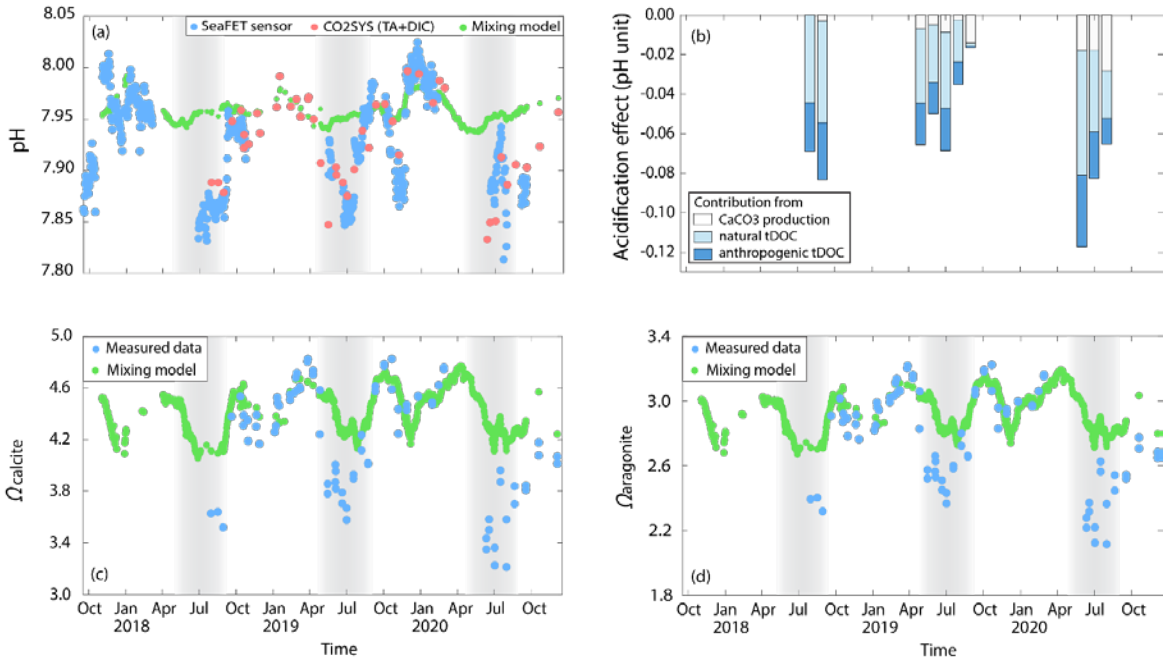

Figure 6. Acidification during the SW Monsoon season (grey shading) due to the extensive remineralization of tDOC. **(a)** Time series of pH from the SeaFET sensor and laboratory measurements of TA and DIC shows reduced pH relative to values expected from conservative mixing during the SW Monsoon. **(b)** Individual contribution to the seasonal acidification from $CaCO_3$ production, remineralization of natural, pre-anthropogenic tDOC, and remineralization of the putative anthropogenic tDOC fraction, based on the results from the mass balance calculations and the reported anthropogenic increase in tDOC export from peatlands (Moore et al. 2013; Yupi et al. 2016). The total acidification effect (height of the stacked bars) is the difference between the measured pH and the predicted value from the conservative mixing model. The results are presented as monthly averages for clarity. **(c – d)** The saturation states of calcite and of aragonite show large decreases compared to the conservative mixing model during the SW Monsoon season.

3.6 Degradability of the peatland-derived tDOC

The tDOC from the peatland-draining Maludam River showed high photo-lability (Fig. 7, Table 3): the DOC concentration decreased first from 3250 µmol L^{-1} to 850 µmol L^{-1} over the course of 525 hours in the solar simulator (Fig. 7a), after which we observed pronounced photo-induced flocculation in the remaining replicates. Although POC was not measured, the quantity

628 of flocs did not visibly decrease during the remaining hours of the experiment, suggesting that
629 photo-flocculated DOC probably remained stable. CDOM a_{350} decreased from 167.4 m^{-1} to 5.9
630 m^{-1}, and the decrease in $SUVA_{254}$ and increase in $S_{275-295}$ indicated the preferential loss of
631 aromatic and high-molecular-weight compounds (Helms et al., 2008; Weishaar et al., 2003)
632 (Fig. 7b–d). The decrease in DOC observed up to 525 hours implies that around 74% of tDOC
633 was labile to photochemical remineralization.
634
635 The experiment in which Maludam River water was exposed to natural sunlight, revealed that
636 photodegradation also resulted in a small but sizable isotopic fractionation (Fig. 7e–h, Table 3).
637 The DOC concentration decreased by 45% from 3069 µmol L^{-1} to 1674 µmol L^{-1}, and $\delta^{13}C_{DOC}$
638 increased from $-31.1‰$ to $-29.9‰$. This implies that the resulting DIC had a $\delta^{13}C$ value of
639 $-32.5‰$, and that photodegradation of this tDOC therefore entailed a fractionation of $-1.4‰$.
640 As in the previous experiment, CDOM and $SUVA_{254}$ decreased strongly, while $S_{275–295}$
641 increased.
642
643 Samples collected from the Singapore Strait during the NE (Fig. 7i–l) and SW Monsoon (Fig.
644 7m–p) both showed pronounced losses of CDOM upon experimental irradiation for >300 hours,
645 but at most small losses of DOC. There was a decrease in a_{350} by >70%, and strong decreases
646 in $SUVA_{254}$ and increases in $S_{275-295}$ during both seasons. However, the NE Monsoon sample
647 showed no change in DOC concentration (Fig. 7i); the SW Monsoon sample only showed a
648 decrease in DOC concentration by 9 µmol L^{-1} (Fig. 7m). Of the bulk DOC in this SW Monsoon

649 sample, 36 μmol L^{-1} was tDOC (estimated from the $\delta^{13}C_{DOC}$). Because the majority of the DOC
650 pool during the NE Monsoon is of marine origin, it appears that the autochthonous marine
651 DOC is not strongly photolabile. Assuming therefore that the observed decrease in DOC in the
652 SW Monsoon experiment was entirely due to tDOC remineralization, our results would
653 indicate that only about 25% (9 out of 36 μmol L^{-1}) of the peatland-derived tDOC that still
654 remains unremineralized in the Singapore Strait is labile to direct photochemical
655 remineralization.
656
657 Moreover, we found that the biodegradability of the SW Monsoon sample from the Singapore
658 Strait was low, with <6% loss of DOC and CDOM a_{350} over the course of the 109-day
659 incubation (Fig. 8). Although the leucine and glucose added as labile carbon to one treatment
660 was rapidly consumed, no additional remineralization of DOC was induced in this treatment.
661 Our results, consistent with the low biodegradability of tDOC from the Maludam River
662 (Nichols & Martin, submitted), suggest that direct microbial remineralization is not a main
663 driver of tDOC remineralization. Whether the observed biodegradation represents loss of tDOC
664 at all or only of autochthonous DOC is unclear.
665
666 In summary, our experiments with the Maludam River samples indicate that around 74% of
667 tDOC is directly photo-mineralizable, while our observational data from the Singapore Strait
668 show that 60–70% of the peatland-derived tDOC is remineralized in the coastal waters of the
669 Sunda Shelf. Our additional experiments then show that of the remaining 30–40% of this tDOC,

<25% is still photo-mineralizable, and that any biodegradation proceeds at most slowly. Depending on how much of the remaining tDOC really is biodegradable, these results imply that possibly around 20–30% of the total peatland tDOC from Sumatra is sufficiently refractory to resist remineralization on the Sunda Shelf and be exported to the Indian Ocean, given that the total water residence time in the Malacca Strait is approximately 2 years (Mayer et al., 2018).

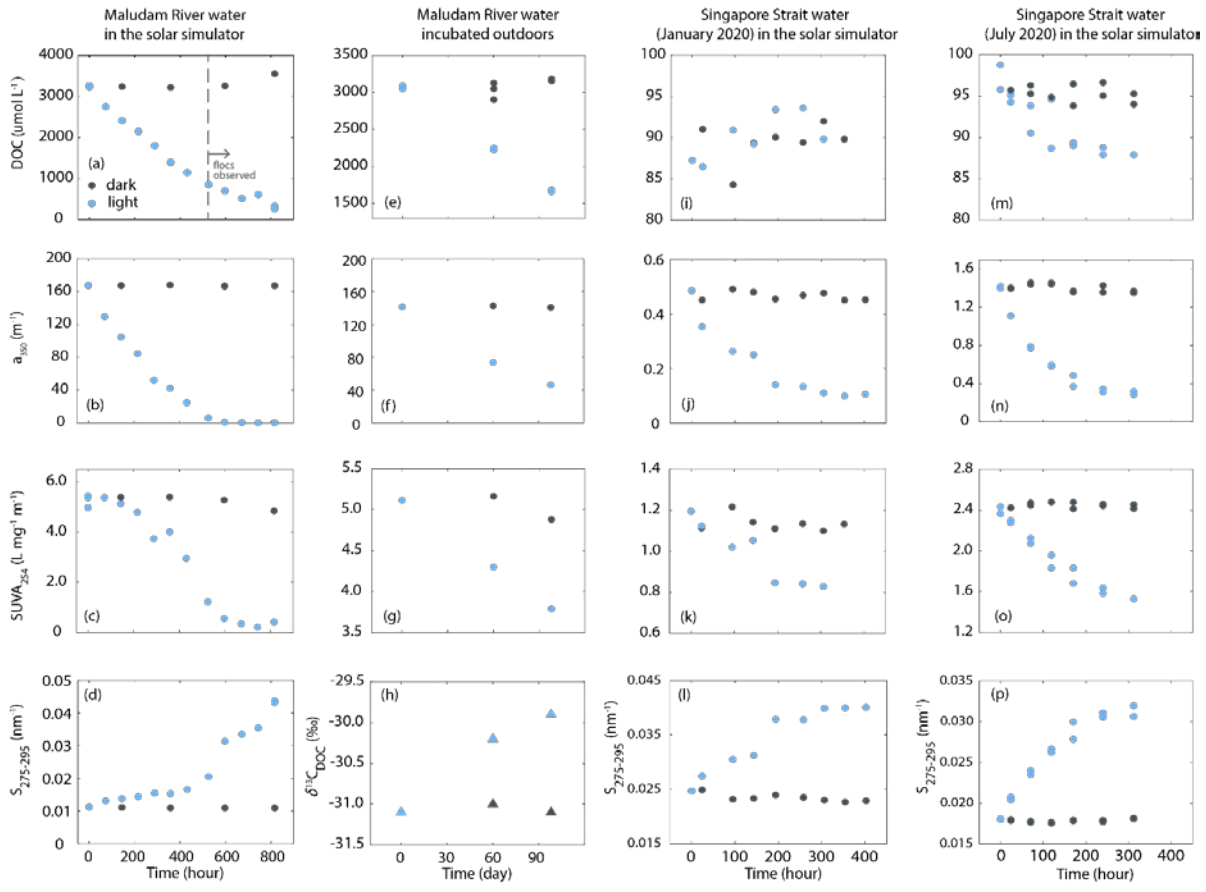

Figure 7. Changes in DOC, CDOM and $\delta^{13}C_{DOC}$ during four photodegradation experiments showing high photo-lability of DOC from the Maludam River but only limited photo-lability from the Singapore Strait. Flocs were observed in the water sample after incubation for 525 hours during the experiment with the Maludam River water in the solar simulator but were not observed in other experiments.

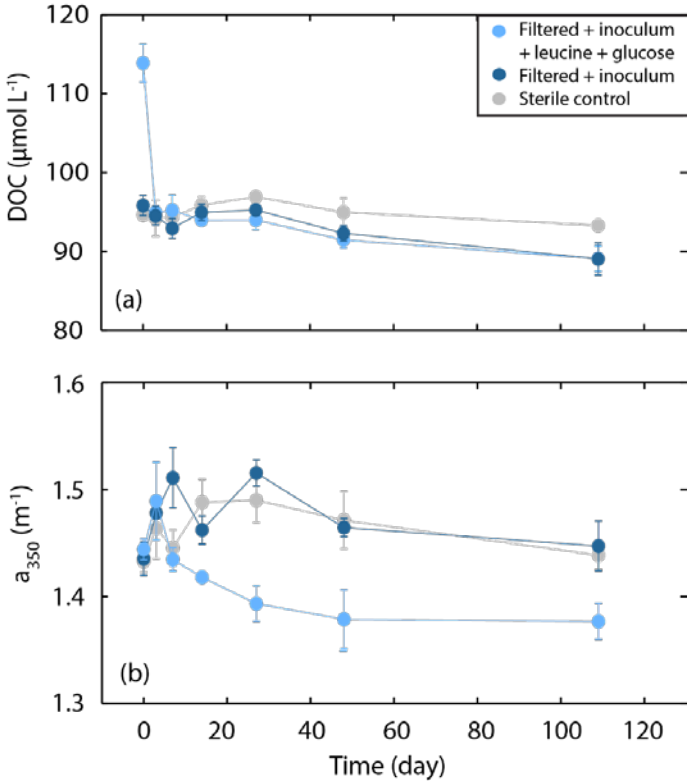

Figure 8. Changes in **(a)** DOC and **(b)** CDOM (a_{350}) during the 109-day incubation showing limited biodegradability of DOC collected from the Singapore Strait.

698 **Table 3. Results of the photodegradation experiments.**

	DOC (μmol L^{-1})	a_{350} (m^{-1})	$S_{275-295}$ (nm^{-1})	$SUVA_{254}$ (L mg^{-1} m^{-1})	$\delta^{13}C_{DOC}$ (‰)	$\delta^{13}C_{DIC}$** (‰)
Maludam River in solar simulator*						
before	3250	167.4	0.011	5.41		
after	850	5.9	0.021	1.23		
%loss	74%	96%				
Maludam River Incubated outdoors						
before	3069	140.88	0.012	5.12	−31.1	-
after	1674	46.41	0.015	3.79	−29.9	−32.5
%loss	45%	67%				
Singapore Strait, NE Monsoon (Jan 2020)						
before	87	0.49	0.025	1.20		
after	89	0.11	0.040	0.83		
%loss	-	78%				
Singapore Strait, SW Monsoon (July 2020)						
before	97	1.40	0.018	2.40		
after	88	0.29	0.032	1.53		
%loss	9%	79%				

699 * Data beyond 525 hours were omitted because flocculation observed.

700 ** δ^{13}C of the DIC produced from remineralization of the initial DOC.

701

702

703

704

705

706

4 Discussions

4.1 Sources and remineralization of tDOC

The correlated seasonal variations of salinity, DOC, $\delta^{13}C_{DOC}$, CDOM absorption and spectral characteristics all indicate that our site receives a large input of tDOC during the SW Monsoon, and a much smaller tDOC input during the NE Monsoon. Although seasonal variation in rainfall can cause variation in tDOC flux from tropical peatlands (Rixen et al., 2016), the variation observed here is driven by the regional advection of coastal water that has mixed with peatland-draining river input according to the monsoon system (Van Maren & Gerritsen, 2012; Mayer & Pohlmann, 2014). The high riverine endmember DOC concentration (892 ± 104 μmol L^{-1}) predicted from the relationship between the total initial tDOC concentration and salinity (Fig. 4f) clearly points to peatlands as the source of the tDOC measured during the SW Monsoon. This seasonally variable advection of peatland tDOC explains the lack of a strong peatland signal in the carbonate system data measured by Hamzah et al. (2020) in the Karimata Strait to the southeast of our site: because they sampled during the SW Monsoon, the peatland-influenced water would have flowed northwards away from their transect and out to the South China Sea.

Our isotope mass balance calculations assume that the seasonal variation in our data is not driven by seasonal changes in autochthonous DOC remineralization. The relatively low chlorophyll-*a* concentrations year-round suggest that autochthonous organic matter production rates are moderate and, importantly, do not show strong seasonality. This is likely due to

728 persistent light limitation caused by strong vertical light attenuation (Chow et al., 2019; Morgan
729 et al., 2020) and tidal mixing of the water column (Mayer & Pohlmann, 2014) which prevents
730 vertical stratification. Moreover, the very small annual range in seawater temperature means
731 that microbial physiological rates will not vary strongly. Therefore, the net community
732 production rate is most likely relatively constant, and we can rule out the possibility that our
733 observations are the result of seasonal changes in production and remineralization of marine
734 autochthonous organic matter. Moreover, the seasonal decrease in $\delta^{13}C_{DIC}$ is too large to be
735 explained by the remineralization of marine DOC with a $\delta^{13}C_{DOC}$ of around $-22‰$. Even
736 though we attributed all the excess DIC to remineralization of tDOC with $\delta^{13}C$ of DIC
737 production of $-32‰$, the depletion in $\delta^{13}C_{DIC}$ was so large that it could only be explained by
738 inferring that an even greater quantity of tDOC had been remineralized and outgassed.
739
740 We further assume that the remineralized terrigenous carbon is tDOC rather than POC. The
741 terrigenous organic carbon in peat-draining rivers in Southeast Asia is overwhelmingly in form
742 of DOC year-round (typically ≥95%) (Alkhatib et al., 2007; Baum et al., 2007; Moore et al.,
743 2011; Müller et al., 2015), and thus any terrigenous POC input is expected to be small in this
744 region. Part of any POC that is delivered by rivers is also likely to sink and accumulate in the
745 sediment, thus decoupling the POC and its remineralization from the water carrying the DOC.
746 Most importantly, the riverine endmember DOC concentration that we infer from our
747 regression of total initial tDOC concentrations *versus* salinity (892 ± 104 μmol L^{-1}) is also very
748 close to the discharge-weighted average DOC concentration measured independently in the

749 main peatland-draining rivers on Sumatra, of 890 ± 159 μmol L^{-1} (Wit et al., 2018). This
750 indicates that additional remineralization of POC is not required to explain the observed
751 variation in DIC and $\delta^{13}C_{DIC}$.
752
753 Remineralization of tDOC can occur either by microbial decomposition (i.e., biodegradation)
754 or by photochemical decomposition. Biodegradation is increasingly recognized as an important
755 pathway of tDOC decomposition in aquatic systems (Tranvik et al., 2009; Ward et al., 2013;
756 Wickland et al., 2007). However, peatland organic matter especially in the tropics is enriched
757 in polyphenolic compounds such as lignin derivatives, which are likely refractory to microbial
758 respiration (Gandois et al., 2014; Hodgkins et al., 2018). Our data showed at most low
759 biodegradability of the tDOC collected from the Singapore Strait, even when amended with
760 labile carbon to stimulate a potential priming effect (Bianchi, 2011; Guenet et al., 2010; van
761 Nugteren et al., 2009). Similarly, freshly collected tDOC from the peatland-draining Maludam
762 River showed at most very limited biodegradability over 50 days, even when amended with
763 dissolved nutrients or mixed into coastal seawater (Nichols and Martin, submitted). In contrast,
764 we found that up to about 74% of peatland-derived tDOC can be photochemically
765 remineralized. This is consistent with previous reports of high photo-lability of tropical
766 peatland tDOC (Gandois et al., 2020; Martin et al., 2018; Spencer et al., 2009). Collectively,
767 these results suggest that photodegradation rather than biodegradation likely drives the
768 observed remineralization.
769

770 It is possible that partial photodegradation increases the biodegradability of the peatland tDOC
771 (Cory & Kling, 2018; Moran et al., 2000; Moran & Zepp, 1997). For example, tDOC
772 processing in Arctic freshwater systems depends on initial photodegradation that stimulates
773 subsequent microbial remineralization (Cory et al., 2014), and 32% of the tDOC
774 remineralization on the Louisiana Shelf was attributed to photochemically stimulated
775 biodegradation (Fichot & Benner, 2014). Our data are consistent with preferential degradation
776 of high-molecular-weight aromatic substances during irradiation, which is believed to increase
777 tDOC biodegradability. Further studies are required to address the importance of
778 photochemical–microbial interactions for Southeast Asian peatland tDOC decomposition.
779
780 Our data showing that the majority of tDOC is remineralized in the Sunda Shelf Sea are
781 consistent with previous work showing that ocean margins are hotspots of tDOC processing
782 (Fichot & Benner, 2014; Kaiser et al., 2017; Kitidis et al., 2019; Painter et al., 2018; Semiletov
783 et al., 2016). This is also comparable to a recent estimate that 63% of Southeast Asian peatland
784 carbon is remineralized, derived by scaling up the estimated sea-to-air CO_2 fluxes in the
785 southern Malacca Strait and Karimata Strait (Wit et al., 2018). This study also inferred that the
786 majority of the remaining tDOC would also be remineralized in the shelf. However, our
787 incubations showed surprisingly low remineralizability of the remaining tDOC reaching our
788 site by microbial and photo-chemical decomposition. Consequently, our data suggest that it is
789 possible that roughly 20–30% of the tDOC from Sumatran peatlands is actually exported to the
790 open Indian Ocean and ultimately contributes to the semi-refractory or even refractory oceanic

DOC pool.

4.2 CO_2 emissions from the Sunda Shelf driven by tDOC remineralization

The mass balance calculations showed that the proportion of the remineralized tDOC that had been removed by CO_2 outgassing increased throughout the SW Monsoon, indicating the ongoing removal of CO_2 to atmosphere. Our estimate that the Singapore Strait contributes a net sea-to-air CO_2 flux of 4.10–8.20 mol C m^{-2} yr^{-1} is consistent with the paradigm that tropical inner shelves tend to act as sources of atmospheric CO_2 (Cai, 2011; Chen et al., 2013; Chen & Borges, 2009). Our estimate is comparable to that of Wit et al. (2018) for the same region (4.12 mol C m^{-2} yr^{-1}), but is much higher than the estimates by Roobaert et al. (2019) (0–0.4 mol C m^{-2} yr^{-1}) and Hamzah et al. (2020) (1.09 mol C m^{-2} yr^{-1}). The estimates of Roobaert et al. (2019) were based on a global data product that lacked direct measurements from the Sunda Shelf Sea, while Hamzah et al. (2020) sampled in the southern Karimata Strait during the SW Monsoon, at which point the peatland tDOC is advected northeastwards into the South China Sea. The fact that the Sunda Shelf is clearly a stronger CO_2 source than estimated by some studies demonstrates the importance of collecting annual time series of carbon biogeochemistry in this region, and of increasing the data coverage for coastal waters in Southeast Asia. Given the potentially sizeable anthropogenic contribution to the peatland tDOC input to the Sunda Shelf, our study further helps to highlight the importance of downstream greenhouse gas emissions from tropical peatland disturbance.

812

813 **4.3 Seasonal acidification driven by tDOC remineralization**

814 During the SW Monsoon, 10–30 μmol kg^{-1} of the remineralized tDOC is still present as DIC
815 upon reaching the Singapore Strait, resulting in seasonal acidification by 0.60–0.10 pH units.
816 Pronounced impacts of tDOC remineralization on the carbonate system were reported for the
817 estuaries and coastal waters of eastern Sumatra (Wit et al., 2018). Our results further show that
818 the seasonal advection of these waters subjects sensitive calcifying communities such as coral
819 reefs, which are found further away from the peatland river estuaries around the islands to the
820 east of Sumatra (UNEP-WCMC, 2010), to pronounced seasonal acidification.

821

822 Ocean acidification, which leads to decrease in the saturation state (Ω) of calcium carbonate,
823 is thought to impair the growth of corals by reducing the calcification rates (Cooper et al., 2008;
824 Langdon, 2005; Pisapia et al., 2019) and skeletal density (Manzello et al., 2008; Mollica et al.,
825 2018), and cause degradation of the coral reefs such as coral bleaching (Anthony et al., 2008;
826 DeCarlo et al., 2017; Fabricius et al., 2011), reduction of coral cover (Gardner et al., 2003;
827 Hughes et al., 2018; Perry et al., 2018) and decrease in coral species diversity (Fabricius et al.,
828 2011). Zero or negative carbonate accretion on coral reefs might be induced when the Ω_{AR}
829 decreases to ~3.3 or below (Hoegh-Guldberg et al., 2007; Kleypas et al., 1999), and large-scale
830 reductions in calcification have been projected for future high-pCO_2 scenarios due to
831 anthropogenic CO_2 emissions (Andersson et al., 2007; Anthony et al., 2008; Dove et al., 2013;
832 Hoegh-Guldberg et al., 2007). The decrease in Ω_{AR} to ~2.7 at our site during the SW Monsoon

might therefore reduce coral calcification and reef development during this period of the year, as has been shown in response to seasonal carbonate system variation in the Great Barrier Reef (Dove et al., 2013; Stoltenberg et al., 2021). Our analysis indicates that the reported increases in tDOC flux after peatland disturbance are sufficiently large to account for a significant part of the observed acidification. This demonstrates that anthropogenic disturbance of tropical peatlands might be impacting sensitive ecosystems such as coral reefs via increased fluvial tDOC export and remineralization.

5 Conclusions

Our results demonstrate that the large input of tDOC from peatlands on Sumatra affects regional DOC concentrations, CO_2 fluxes, and the carbonate system in the Sunda Shelf Sea. Isotope mass balance calculations indicate that 60–70% of this tDOC is remineralized in the coastal waters of shelf sea close to the peatlands, and incubation experiments suggest that photodegradation drives a major part of this remineralization. The increase in DIC concentration caused by this remineralization results in a seasonal decrease in seawater pH by up to 0.10 units, of which the remineralization of the putative anthropogenic tDOC fraction might account for a pH reduction of 0.01–0.04 units, potentially impacting coral physiology in the region. Most of the CO_2 produced from this tDOC remineralization is likely eventually lost to the atmosphere. Our data thus provide further evidence that there is a large indirect pathway of CO_2 emissions due to peatland disturbance via the remineralization of tDOC in coastal seas. Despite this rapid remineralization of a large fraction of tDOC, we also found low degradability of the residual tDOC pool. We conclude that the Sunda Shelf is an efficient sink of peatland-derived tDOC and a significant source of atmospheric CO_2, but that a higher proportion of the peatland tDOC might be refractory and exported to the Indian Ocean than was previously thought. The long-term fate of this tDOC flux to the open ocean remains uncertain.

Acknowledgements

We thank Molly Moynihan, Nikita Kaushal, Robert Nichols, Ashleen Tan Su Ying, Chen Shuang, Woo Oon Yee, Kyle Morgan and Phyllis Kho Yu Yi for help during field work and laboratory analysis. We are very grateful to Nikita Kaushal for measuring $\delta^{13}C_{DIC}$, to Nathalie Goodkin for providing the moored CTD and pH sensors for this work, to Evelyn Lim for performing some of the photodegradation experiments, to Moritz Müller for collecting water samples from the Maludam River, and to Francis Yeo, Sapari and Surpato of *Dolphin Explorer* for enabling the sample collection. This research was funded by the National Research Foundation Singapore, Prime Minister's Office, as part of the Marine Science Research and Development Programme through grant MSRDP-P32 to P.M., and forms part of the Ph.D. research of Y.Z.

Author Contributions

P.M. conceptualized the research and acquired funding; Y.Z., Y.C., K.Y.W.C. and P.M. conducted field work; Y.Z. and Y.C. conducted degradation experiments; Y.Z., Y.C. and K.Y.W.C. analyzed samples; Y.Z. analyzed the data with support from C.D.E., P.M., Y.C. and K.Y.W.C.; Y.Z., P.M., C.D.E. and Y.C. wrote the manuscript. All authors edited the manuscript and approved the final version.

Competing Interests

None of the authors have competing interests to declare.

Data availability

All processed data are available in the Supplementary Data Table. All raw data files and analysis codes will be made available through the Nanyang Technological University Data Repository upon acceptance, under doi:10.21979/N9/MVYDRU.

Materials & Correspondence

Correspondence and request for materials should be addressed to Yongli Zhou: zhou0303@e.ntu.edu.sg or Patrick Martin: pmartin@ntu.edu.sg.

References

Alkhatib, M., Jennerjahn, T. C., & Samiaji, J. (2007). Biogeochemistry of the Dumai River estuary, Sumatra, Indonesia, a tropical blackwater river. *Limnology and Oceanography*, *52*(6), 2410–2417. https://doi.org/10.4319/lo.2007.52.6.2410

Alling, V., Humborg, C., Mörth, C.-M., Rahm, L., & Pollehne, F. (2008). Tracing terrestrial organic matter by δ^{34} S and δ^{13}C signatures in a subarctic estuary. *Limnology and Oceanography*, *53*(6), 2594–2602. https://doi.org/10.4319/lo.2008.53.6.2594

Andersson, A. J., Bates, N. R., & Mackenzie, F. T. (2007). Dissolution of carbonate sediments under rising pCO_2 and ocean acidification: Observations from Devil's Hole, Bermuda. *Aquatic Geochemistry*, *13*(3), 237–264. https://doi.org/10.1007/s10498-007-9018-8

Anthony, K. R. N., Kline, D. I., Diaz-Pulido, G., Dove, S., & Hoegh-Guldberg, O. (2008). Ocean acidification causes bleaching and productivity loss in coral reef builders. *Proceedings of the National Academy of Sciences of the United States of America*, *105*(45), 17442–17446. https://doi.org/10.1073/pnas.0804478105

Assayag, N., Rivé, K., Ader, M., Jézéquel, D., & Agrinier, P. (2006). Improved method for isotopic and quantitative analysis of dissolved inorganic carbon in natural water samples. *Rapid Communications in Mass Spectrometry*, *20*(15), 2243–2251. https://doi.org/10.1002/rcm.2585

Baum, A. (2008). Tropical blackwater biogeochemistry : The Siak River in Central Sumatra , Indonesia. *PhD Thesis, University of Bremen, Bremen, Germany*.

Baum, A., Rixen, T., & Samiaji, J. (2007). Relevance of peat draining rivers in central Sumatra for the riverine input of dissolved organic carbon into the ocean. *Estuarine, Coastal and Shelf Science*, *73*(3–4), 563–570. https://doi.org/10.1016/j.ecss.2007.02.012

Bauman, A. G., Hoey, A. S., Dunshea, G., Feary, D. A., Low, J., & Todd, P. A. (2017). Macroalgal browsing on a heavily degraded, urbanized equatorial reef system. *Scientific Reports*, *7*(1), 1–8. https://doi.org/10.1038/s41598-017-08873-3

Beleites, C., & Sergo, V. (2012). hyperSpec: a package to handle hyperspectral data sets in R. *Journal of Statistical Software*.

Bianchi, T. S. (2011). The role of terrestrially derived organic carbon in the coastal ocean: A changing paradigm and the priming effect. *Proceedings of the National Academy of Sciences*, *108*(49), 19473–19481. https://doi.org/10.1073/pnas.1017982108

939 Cai, W.-J. (2011). Estuarine and Coastal Ocean Carbon Paradox: CO_2 Sinks or Sites of
940 Terrestrial Carbon Incineration? *Annual Review of Marine Science*, *3*(1), 123–145.
941 https://doi.org/10.1146/annurev-marine-120709-142723
942 Cao, X., Aiken, G. R., Butler, K. D., Huntington, T. G., Balch, W. M., Mao, J., & Schmidt-
943 Rohr, K. (2018). Evidence for major input of riverine organic matter into the ocean.
944 *Organic Geochemistry*, *116*, 62–76. https://doi.org/10.1016/j.orggeochem.2017.11.001
945 Chen, C.-T. A., & Borges, A. V. (2009). Reconciling opposing views on carbon cycling in
946 the coastal ocean: Continental shelves as sinks and near-shore ecosystems as sources of
947 atmospheric CO_2. *Deep Sea Research Part II: Topical Studies in Oceanography*, *56*(8–
948 10), 578–590. https://doi.org/10.1016/j.dsr2.2009.01.001
949 Chen, C.-T. A., Huang, T.-H., Chen, Y.-C., Bai, Y., He, X., & Kang, Y. (2013). Air–sea
950 exchanges of CO_2 in the world's coastal seas. *Biogeosciences*, *10*(10), 6509–6544.
951 https://doi.org/10.5194/bg-10-6509-2013
952 Cheng, L., Normandeau, C., Bowden, R., Doucett, R., Gallagher, B., Gillikin, D. P., et al.
953 (2019). An international intercomparison of stable carbon isotope composition
954 measurements of dissolved inorganic carbon in seawater. *Limnology and*
955 *Oceanography: Methods*, *17*(3), 200–209. https://doi.org/10.1002/lom3.10300
956 Chow, G. S. E., Chan, Y. K. S., Jain, S. S., & Huang, D. (2019). Light limitation selects for
957 depth generalists in urbanised reef coral communities. *Marine Environmental Research*,
958 *147*(February), 101–112. https://doi.org/10.1016/j.marenvres.2019.04.010
959 Chupakova, A. A., Chupakov, A. V., Neverova, N. V., Shirokova, L. S., & Pokrovsky, O. S.

(2018). Photodegradation of river dissolved organic matter and trace metals in the largest European Arctic estuary. *Science of The Total Environment*, *622–623*, 1343–1352. https://doi.org/10.1016/j.scitotenv.2017.12.030

Cooper, T. F., De'ath, G., Fabricius, K. E., & Lough, J. M. (2008). Declining coral calcification in massive Porites in two nearshore regions of the northern Great Barrier Reef. *Global Change Biology*, *14*(3), 529–538. https://doi.org/10.1111/j.1365-2486.2007.01520.x

Cory, R. M., & Kling, G. W. (2018). Interactions between sunlight and microorganisms influence dissolved organic matter degradation along the aquatic continuum. *Limnology and Oceanography Letters*. https://doi.org/10.1002/lol2.10060

Cory, R. M., Ward, C. P., Crump, R. C., & Kling, G. W. (2014). Sunlight controls water column processing of carbon in arctic fresh waters, *345*(6199).

CYGNSS. (2017). CYGNSS Level 2 Science Data Record Version 2.1. NASA Physical Oceanography DAAC. https://doi.org/10.5067/CYGNS-L2X21

DeCarlo, T. M., Cohen, A. L., Wong, G. T. F., Shiah, F.-K., Lentz, S. J., Davis, K. A., et al. (2017). Community production modulates coral reef pH and the sensitivity of ecosystem calcification to ocean acidification. *Journal of Geophysical Research: Oceans*, *122*(1), 745–761. https://doi.org/10.1002/2016JC012326

Dommain, R., Couwenberg, J., Glaser, P. H., Joosten, H., & Suryadiputra, I. N. N. (2014). Carbon storage and release in Indonesian peatlands since the last deglaciation. *Quaternary Science Reviews*, *97*, 1–32. https://doi.org/10.1016/j.quascirev.2014.05.002

981 Dove, S. G., Kline, D. I., Pantos, O., Angly, F. E., Tyson, G. W., & Hoegh-Guldberg, O.
982 (2013). Future reef decalcification under a business-as-usual CO_2 emission scenario.
983 *Proceedings of the National Academy of Sciences of the United States of America*,
984 *110*(38), 15342–15347. https://doi.org/10.1073/pnas.1302701110
985 Evans, C. D., Page, S. E., Jones, T., Moore, S., Gauci, V., Laiho, R., et al. (2014).
986 Contrasting vulnerability of drained tropical and high-latitude peatlands to fluvial loss of
987 stored carbon. *Global Biogeochemical Cycles*, *28*(11), 1215–1234.
988 https://doi.org/10.1002/2013GB004782
989 Fabricius, K. E., Langdon, C., Uthicke, S., Humphrey, C., Noonan, S., De'ath, G., et al.
990 (2011). Losers and winners in coral reefs acclimatized to elevated carbon dioxide
991 concentrations. *Nature Climate Change*, *1*(3), 165–169.
992 https://doi.org/10.1038/nclimate1122
993 Fichot, C. G., & Benner, R. (2014). The fate of terrigenous dissolved organic carbon in a
994 river-influenced ocean margin. *Global Biogeochemical Cycles*, *28*(3), 300–318.
995 https://doi.org/10.1002/2013GB004670
996 Follett, C. L., Repeta, D. J., Rothman, D. H., Xu, L., & Santinelli, C. (2014). Hidden cycle of
997 dissolved organic carbon in the deep ocean. *Proceedings of the National Academy of*
998 *Sciences of the United States of America*, *111*(47), 16706–16711.
999 https://doi.org/10.1073/pnas.1407445111
1000 Gandois, L., Teisserenc, R., Cobb, A. R., Chieng, H. I., Lim, L. B. L., Kamariah, A. S., et al.
1001 (2014). Origin, composition, and transformation of dissolved organic matter in tropical

1002 peatlands. *Geochimica et Cosmochimica Acta*, *137*, 35–47.
1003 https://doi.org/10.1016/j.gca.2014.03.012
1004 Gandois, L., Hoyt, A. M., Mounier, S., Le Roux, G., Harvey, C. F., Claustres, A., et al.
1005 (2020). From canals to the coast: dissolved organic matter and trace metal composition
1006 in rivers draining degraded tropical peatlands in Indonesia. *Biogeosciences*, *17*(7),
1007 1897–1909. https://doi.org/10.5194/bg-17-1897-2020
1008 Gardner, T. A., Côté, I. M., Gill, J. A., Grant, A., & Watkinson, A. R. (2003). Long-term
1009 region-wide declines in Caribbean corals. *Science*, *301*(5635), 958–960.
1010 https://doi.org/10.1126/science.1086050
1011 Gordon, A. L., Huber, B. A., Metzger, E. J., Susanto, R. D., Hurlburt, H. E., & Adi, T. R.
1012 (2012). South China Sea throughflow impact on the Indonesian throughflow.
1013 *Geophysical Research Letters*, *39*(11), 1–7. https://doi.org/10.1029/2012GL052021
1014 Gran, G. (1952). Determination of the equivalence point in potentiometric titrations. Part II.
1015 *The Analyst*. https://doi.org/10.1039/AN9527700661
1016 Guenet, B., Danger, M., Abbadie, L., & Lacroix, G. (2010). Priming effect: bridging the gap
1017 between terrestrial and aquatic ecology. *Ecology*, *91*(10), 2850–2861.
1018 https://doi.org/10.1890/09-1968.1
1019 Hamzah, F., Agustiadi, T., Susanto, R. D., Wei, Z., Guo, L., Cao, Z., & Dai, M. (2020).
1020 Dynamics of the Carbonate System in the Western Indonesian Seas During the
1021 Southeast Monsoon. *Journal of Geophysical Research: Oceans*, *125*(1), 1–18.
1022 https://doi.org/10.1029/2018JC014912

1023 Helms, J. R., Stubbins, A., Ritchie, J. D., Minor, E. C., Kieber, D. J., & Mopper, K. (2008).
1024 Absorption spectral slopes and slope ratios as indicators of molecular weight, source,
1025 and photobleaching of chromophoric dissolved organic matter. *Limnology and*
1026 *Oceanography*, *53*(3), 955–969. https://doi.org/10.4319/lo.2008.53.3.0955
1027 van Heuven, S., Pierrot, D., Rae, J. W. B., Lewis, E., & Wallace, D. W. R. (2011). MATLAB
1028 Program Developed for CO_2 System Calculations. ORNL/CDIAC-105b. *ORNL/CDIAC-*
1029 *105b. Carbon Dioxide Information Analysis Center, Oak Ridge National Laboratory,*
1030 *U.S. Department of Energy, Oak Ridge, Tennessee*.
1031 https://doi.org/10.3334/CDIAC/otg.CO2SYS_MATLAB_v1.1
1032 Hodgkins, S. B., Richardson, C. J., Dommain, R., Wang, H., Glaser, P. H., Verbeke, B., et al.
1033 (2018). Tropical peatland carbon storage linked to global latitudinal trends in peat
1034 recalcitrance. *Nature Communications*, *9*(1), 1–13. https://doi.org/10.1038/s41467-018-
1035 06050-2
1036 Hoegh-Guldberg, O., Mumby, P. J., Hooten, A. J., Steneck, R. S., Greenfield, P., Gomez, E.,
1037 et al. (2007). Coral Reefs Under Rapid Climate Change and Ocean Acidification.
1038 *Science*, *318*(5857), 1737–1742. https://doi.org/10.1126/science.1152509
1039 Huang, D., Tun, K. P. P., Chou, L. M., & Todd, P. a. (2009). An inventory of zooxanthellate
1040 scleractinian corals in Singapore, including 33 new records. *Raffles Bulletin of Zoology*,
1041 *22*(22), 69–80. Retrieved from http://rmbr.nus.edu.sg/rbz/biblio/s22/s22rbz069-080.pdf
1042 Hughes, T. P., Kerry, J. T., Baird, A. H., Connolly, S. R., Dietzel, A., Eakin, C. M., et al.
1043 (2018). Global warming transforms coral reef assemblages. *Nature*, *556*(7702), 492–

496. https://doi.org/10.1038/s41586-018-0041-2

Humborg, C., Geibel, M. C., Anderson, L. G., Björk, G., Mörth, C.-M., Sundbom, M., et al. (2017). Sea-air exchange patterns along the central and outer East Siberian Arctic Shelf as inferred from continuous CO_2 , stable isotope, and bulk chemistry measurements. *Global Biogeochemical Cycles*, *31*(7), 1173–1191. https://doi.org/10.1002/2017GB005656

Humphreys, M. P., Greatrix, F. M., Tynan, E., Achterberg, E. P., Griffiths, A. M., Fry, C. H., et al. (2016). Stable carbon isotopes of dissolved inorganic carbon for a zonal transect across the subpolar North Atlantic Ocean in summer 2014. *Earth System Science Data*, *8*(1), 221–233. https://doi.org/10.5194/essd-8-221-2016

Januchowski-Hartley, F. A., Bauman, A. G., Morgan, K. M., Seah, J. C. L., Huang, D., & Todd, P. A. (2020). Accreting coral reefs in a highly urbanized environment. *Coral Reefs*, *39*(3), 717–731. https://doi.org/10.1007/s00338-020-01953-3

Kaiser, K., Benner, R., & Amon, R. M. W. (2017). The fate of terrigenous dissolved organic carbon on the Eurasian shelves and export to the North Atlantic. *Journal of Geophysical Research: Oceans*, *122*(1), 4–22. https://doi.org/10.1002/2016JC012380

Kitidis, V., Shutler, J. D., Ashton, I., Warren, M., Brown, I., Findlay, H., et al. (2019). Winter weather controls net influx of atmospheric CO_2 on the north-west European shelf. *Scientific Reports*, *9*(1), 1–11. https://doi.org/10.1038/s41598-019-56363-5

Kleypas, J. A., McManu, J. W., & Mene, L. A. B. (1999). Environmental limits to coral reef development: Where do we draw the line? *American Zoologist*, *39*(1), 146–159.

https://doi.org/10.1093/icb/39.1.146

Langdon, C. (2005). Effect of elevated pCO_2 on photosynthesis and calcification of corals and interactions with seasonal change in temperature/irradiance and nutrient enrichment. *Journal of Geophysical Research*, *110*(C9), C09S07. https://doi.org/10.1029/2004JC002576

Letscher, R. T., Hansell, D. A., & Kadko, D. (2011). Rapid removal of terrigenous dissolved organic carbon over the Eurasian shelves of the Arctic Ocean. *Marine Chemistry*, *123*(1–4), 78–87. https://doi.org/10.1016/j.marchem.2010.10.002

Lønborg, C., Calleja, M. L., Fabricius, K. E., Smith, J. N., & Achterberg, E. P. (2019). The Great Barrier Reef: A source of CO_2 to the atmosphere. *Marine Chemistry*, *210*, 24–33. https://doi.org/10.1016/j.marchem.2019.02.003

Manzello, D. P., Kleypas, J. A., Budd, D. A., Eakin, C. M., Glynn, P. W., & Langdon, C. (2008). Poorly cemented coral reefs of the eastern tropical Pacific: Possible insights into reef development in a high-CO_2 world. *Proceedings of the National Academy of Sciences*, *105*(30), 10450–10455. https://doi.org/10.1073/pnas.0712167105

Van Maren, D. S., & Gerritsen, H. (2012). Residual flow and tidal asymmetry in the Singapore Strait, with implications for resuspension and residual transport of sediment. *Journal of Geophysical Research: Oceans*, *117*(4), 1–18. https://doi.org/10.1029/2011JC007615

Martin, P., Cherukuru, N., Tan, A. S. Y., Sanwlani, N., Mujahid, A., & Müller, M. (2018). Distribution and cycling of terrigenous dissolved organic carbon in peatland-draining

1086 rivers and coastal waters of Sarawak, Borneo. *Biogeosciences*, *15*(22), 6847–6865.
1087 https://doi.org/10.5194/bg-15-6847-2018
1088 Mayer, B., & Pohlmann, T. (2014). Simulation of organic pollutants: First step towards an
1089 adaptation to the malacca strait. *Asian Journal of Water, Environment and Pollution,*
1090 *11*(1), 75–86.
1091 Mayer, B., Rixen, T., & Pohlmann, T. (2018). The spatial and temporal variability of air-sea
1092 CO_2 fluxes and the effect of net coral reef calcification in the Indonesian Seas: A
1093 numerical sensitivity study. *Frontiers in Marine Science*, *5*(APR), 1–19.
1094 https://doi.org/10.3389/fmars.2018.00116
1095 Medeiros, P. M., Seidel, M., Ward, N. D., Carpenter, E. J., Gomes, H. R., Niggemann, J., et
1096 al. (2015). Fate of the Amazon River dissolved organic matter in the tropical Atlantic
1097 Ocean. *Global Biogeochemical Cycles*, *29*(5), 677–690.
1098 https://doi.org/10.1002/2015GB005115
1099 Medeiros, P. M., Seidel, M., Niggemann, J., Spencer, R. G. M., Hernes, P. J., Yager, P. L., et
1100 al. (2016). A novel molecular approach for tracing terrigenous dissolved organic matter
1101 into the deep ocean. *Global Biogeochemical Cycles*, *30*(5), 689–699.
1102 https://doi.org/10.1002/2015GB005320
1103 Meybeck, M. (1982). Carbon, nitrogen, and phosphorus transport by world rivers. *American*
1104 *Journal of Science*, *282*(4), 401–450. https://doi.org/10.2475/ajs.282.4.401
1105 Meyers-Schulte, K. J., & Hedges, J. I. (1986). Molecular evidence for a terrestrial component
1106 of organic matter dissolved in ocean water. *Nature*, *321*(6065), 61–63.

https://doi.org/10.1038/321061a0

Miettinen, J., Shi, C., & Liew, S. C. (2016). Land cover distribution in the peatlands of Peninsular Malaysia, Sumatra and Borneo in 2015 with changes since 1990. *Global Ecology and Conservation*, *6*, 67–78. https://doi.org/10.1016/j.gecco.2016.02.004

Mollica, N. R., Guo, W., Cohen, A. L., Huang, K. F., Foster, G. L., Donald, H. K., & Solow, A. R. (2018). Ocean acidification affects coral growth by reducing skeletal density. *Proceedings of the National Academy of Sciences of the United States of America*, *115*(8), 1754–1759. https://doi.org/10.1073/pnas.1712806115

Moore, S., Gauci, V., Evans, C. D., & Page, S. E. (2011). Fluvial organic carbon losses from a Bornean blackwater river. *Biogeosciences*, *8*(4), 901–909. https://doi.org/10.5194/bg-8-901-2011

Moore, S., Evans, C. D., Page, S. E., Garnett, M. H., Jones, T. G., Freeman, C., et al. (2013). Deep instability of deforested tropical peatlands revealed by fluvial organic carbon fluxes. *Nature*, *493*(7434), 660–663. https://doi.org/10.1038/nature11818

Moran, M. A., & Zepp, R. G. (1997). Role of photoreactions in the formation of biologically labile compounds from dissolved organic matter. *Limnology and Oceanography*, *42*(6), 1307–1316. https://doi.org/10.4319/lo.1997.42.6.1307

Moran, M. A., Sheldon, W. M., & Zepp, R. G. (2000). Carbon loss and optical property changes during long-term photochemical and biological degradation of estuarine dissolved organic matter. *Limnology and Oceanography*, *45*(6), 1254–1264. https://doi.org/10.4319/lo.2000.45.6.1254

1128 Morgan, K. M., Moynihan, M. A., Sanwlani, N., & Switzer, A. D. (2020). Light Limitation
1129 and Depth-Variable Sedimentation Drives Vertical Reef Compression on Turbid Coral
1130 Reefs. *Frontiers in Marine Science*, *7*(November), 1–13.
1131 https://doi.org/10.3389/fmars.2020.571256
1132 Müller-Dum, D., Warneke, T., Rixen, T., Müller, M., Baum, A., Christodoulou, A., et al.
1133 (2019). Impact of peatlands on carbon dioxide (CO_2) emissions from the Rajang River
1134 and Estuary, Malaysia. *Biogeosciences*, *16*(1), 17–32. https://doi.org/10.5194/bg-16-17-
1135 2019
1136 Müller, D., Warneke, T., Rixen, T., Müller, M., Jamahari, S., Denis, N., et al. (2015). Lateral
1137 carbon fluxes and CO_2 outgassing from a tropical peat-draining river. *Biogeosciences*,
1138 *12*(20), 5967–5979. https://doi.org/10.5194/bg-12-5967-2015
1139 van Nugteren, P., Moodley, L., Brummer, G. J., Heip, C. H. R., Herman, P. M. J., &
1140 Middelburg, J. J. (2009). Seafloor ecosystem functioning: The importance of organic
1141 matter priming. *Marine Biology*, *156*(11), 2277–2287. https://doi.org/10.1007/s00227-
1142 009-1255-5
1143 Opsahl, S., & Benner, R. (1997). Distribution and cycling of terrigenous dissolved organic
1144 matter in the ocean. *Nature*, *386*(6624), 480–482. https://doi.org/10.1038/386480a0
1145 Opsahl, S., & Zepp, R. G. (2001). Photochemically-induced alteration of stable carbon
1146 isotope ratios (δ13C) in terrigeneous dissolved organic carbon. *Geophysical Research*
1147 *Letters*, *28*(12), 2417–2420. https://doi.org/10.1029/2000GL012686
1148 Osburn, C. L., Morris, D. P., Thorn, K. A., & Moeller, R. E. (2001). Chemical and optical

changes in freshwater dissolved organic matter exposed to solar radiation. *Biogeochemistry*, *54*(3), 251–278. https://doi.org/10.1023/A:1010657428418

Page, S. E., Rieley, J. O., & Banks, C. J. (2011). Global and regional importance of the tropical peatland carbon pool. *Global Change Biology*, *17*(2), 798–818. https://doi.org/10.1111/j.1365-2486.2010.02279.x

Painter, S. C., Lapworth, D. J., Woodward, E. M. S., Kroeger, S., Evans, C. D., Mayor, D. J., & Sanders, R. J. (2018). Terrestrial dissolved organic matter distribution in the North Sea. *Science of the Total Environment*, *630*, 630–647. https://doi.org/10.1016/j.scitotenv.2018.02.237

Perry, C. T., Alvarez-Filip, L., Graham, N. A. J., Mumby, P. J., Wilson, S. K., Kench, P. S., et al. (2018). Loss of coral reef growth capacity to track future increases in sea level. *Nature*, *558*(7710), 396–400. https://doi.org/10.1038/s41586-018-0194-z

Pisapia, C., Hochberg, E. J., & Carpenter, R. (2019). Multi-Decadal Change in Reef-Scale Production and Calcification Associated With Recent Disturbances on a Lizard Island Reef Flat. *Frontiers in Marine Science*, *6*(September), 1–10. https://doi.org/10.3389/fmars.2019.00575

Rixen, T., Baum, A., Pohlmann, T., Balzer, W., Samiaji, J., & Jose, C. (2008). The Siak, a tropical black water river in central Sumatra on the verge of anoxia. *Biogeochemistry*, *90*(2), 129–140. https://doi.org/10.1007/s10533-008-9239-y

Rixen, T., Baum, A., Wit, F., & Samiaji, J. (2016). Carbon leaching from tropical peat soils and consequences for carbon balances. *Frontiers in Earth Science*, *4*(July).

https://doi.org/10.3389/feart.2016.00074

Roobaert, A., Laruelle, G. G., Landschützer, P., Gruber, N., Chou, L., & Regnier, P. (2019). The Spatiotemporal Dynamics of the Sources and Sinks of CO_2 in the Global Coastal Ocean. *Global Biogeochemical Cycles*, *2*, 1–22. https://doi.org/10.1029/2019GB006239

Ruf, C. S., Gleason, S., & McKague, D. S. (2019). Assessment of CYGNSS Wind Speed Retrieval Uncertainty. *IEEE Journal of Selected Topics in Applied Earth Observations and Remote Sensing*, *12*(1), 87–97. https://doi.org/10.1109/JSTARS.2018.2825948

Samanta, S., Dalai, T. K., Pattanaik, J. K., Rai, S. K., & Mazumdar, A. (2015). Dissolved inorganic carbon (DIC) and its $\delta^{13}C$ in the Ganga (Hooghly) River estuary, India: Evidence of DIC generation via organic carbon degradation and carbonate dissolution. *Geochimica et Cosmochimica Acta*, *165*, 226–248. https://doi.org/10.1016/j.gca.2015.05.040

Semiletov, I., Pipko, I., Gustafsson, Ö., Anderson, L. G., Sergienko, V., Pugach, S., et al. (2016). Acidification of East Siberian Arctic Shelf waters through addition of freshwater and terrestrial carbon. *Nature Geoscience*, *9*(5), 361–365. https://doi.org/10.1038/NEGO2695

Shirokova, L. S., Chupakov, A. V., Zabelina, S. A., Neverova, N. V., Payandi-Rolland, D., Causserand, C., et al. (2019). Humic surface waters of frozen peat bogs (permafrost zone) are highly resistant to bio- and photodegradation. *Biogeosciences*, *16*(12), 2511–2526. https://doi.org/10.5194/bg-16-2511-2019

Siegel, H., Gerth, M., Stottmeister, I., Baum, A., & Samiaji, J. (2019). Remote Sensing of

1191 Coastal Discharge of SE Sumatra (Indonesia). In *Remote Sensing of the Asian Seas* (pp.
1192 359–376). Cham: Springer International Publishing. https://doi.org/10.1007/978-3-319-
1193 94067-0_20
1194 Spencer, R. G. M., Stubbins, A., Hernes, P. J., Baker, A., Mopper, K., Aufdenkampe, A. K.,
1195 et al. (2009). Photochemical degradation of dissolved organic matter and dissolved
1196 lignin phenols from the Congo River. *Journal of Geophysical Research*, *114*(G03010).
1197 https://doi.org/10.1029/2009JG000968
1198 Stoltenberg, L., Schulz, K. G., Lantz, C. A., Cyronak, T., & Eyre, B. D. (2021). Late
1199 afternoon seasonal transition to dissolution in a coral reef: An early warning of a net
1200 dissolving ecosystem? *Geophysical Research Letters*.
1201 https://doi.org/10.1029/2020gl090811
1202 Stubbins, A., Mann, P. J., Powers, L., Bittar, T. B., Dittmar, T., McIntyre, C. P., et al. (2017).
1203 Low photolability of yedoma permafrost dissolved organic carbon. *Journal of*
1204 *Geophysical Research: Biogeosciences*, *122*(1), 200–211.
1205 https://doi.org/10.1002/2016JG003688
1206 Tranvik, L. J., Downing, J. A., Cotner, J. B., Loiselle, S. A., Striegl, R. G., Ballatore, T. J., et
1207 al. (2009). Lakes and reservoirs as regulators of carbon cycling and climate. *Limnology*
1208 *and Oceanography*, *54*(6part2), 2298–2314.
1209 https://doi.org/10.4319/lo.2009.54.6_part_2.2298
1210 UNEP-WCMC. (2010). Global distribution of warm-water coral reefs, compiled from
1211 multiple sources including the Millennium Coral Reef Mapping Project, Version 1.3.

1212 Wanninkhof, R. (1992). Relationship between wind speed and gas exchange over the ocean.
1213 *Journal of Geophysical Research*, *97*(C5), 7373. https://doi.org/10.1029/92JC00188
1214 Wanninkhof, R., Asher, W. E., Ho, D. T., Sweeney, C., & McGillis, W. R. (2009). Advances
1215 in Quantifying Air-Sea Gas Exchange and Environmental Forcing. *Annual Review of*
1216 *Marine Science*, *1*(1), 213–244. https://doi.org/10.1146/annurev.marine.010908.163742
1217 Ward, N. D., Keil, R. G., Medeiros, P. M., Brito, D. C., Cunha, A. C., Dittmar, T., et al.
1218 (2013). Degradation of terrestrially derived macromolecules in the Amazon River.
1219 *Nature Geoscience*, *6*(7), 530–533. https://doi.org/10.1038/ngeo1817
1220 Weishaar, J. L., Aiken, G. R., Bergamaschi, B. A., Fram, M. S., Fujii, R., & Mopper, K.
1221 (2003). Evaluation of Specific Ultraviolet Absorbance as an Indicator of the Chemical
1222 Composition and Reactivity of Dissolved Organic Carbon. *Environmental Science &*
1223 *Technology*, *37*(20), 4702–4708. https://doi.org/10.1021/es030360x
1224 Weiss, R. F. (1974). Carbon dioxide in water and seawater: the solubility of a non-ideal gas.
1225 *Marine Chemistry*, *2*(3), 203–215. https://doi.org/10.1016/0304-4203(74)90015-2
1226 Welschmeyer, N. A. (1994). Fluorometric analysis of chlorophyll a in the presence of
1227 chlorophyll b and pheopigments. *Limnology and Oceanography*, *39*(8), 1985–1992.
1228 https://doi.org/10.4319/lo.1994.39.8.1985
1229 Wickland, K. P., Neff, J. C., & Aiken, G. R. (2007). Dissolved organic carbon in Alaskan
1230 boreal forest: Sources, chemical characteristics, and biodegradability. *Ecosystems*, *10*(8),
1231 1323–1340. https://doi.org/10.1007/s10021-007-9101-4
1232 Wit, F., Müller, D., Baum, A., Warneke, T., Pranowo, W. S., Müller, M., & Rixen, T. (2015).

1233 The impact of disturbed peatlands on river outgassing in Southeast Asia. *Nature*
1234 *Communications*, *6*, 10155. https://doi.org/10.1038/ncomms10155
1235 Wit, F., Rixen, T., Baum, A., Pranowo, W. S., & Hutahaean, A. A. (2018). The Invisible
1236 Carbon Footprint as a hidden impact of peatland degradation inducing marine carbonate
1237 dissolution in Sumatra, Indonesia. *Scientific Reports*, *8*(1), 17403.
1238 https://doi.org/10.1038/s41598-018-35769-7
1239 Yupi, H. M., Inoue, T., Bathgate, J., & Putra, R. (2016). Concentrations, loads and yields of
1240 organic carbon from two tropical peat swamp forest streams in Riau province, Sumatra,
1241 Indonesia. *Mires and Peat*, *18*, 1–15. https://doi.org/10.19189/MaP.2015.OMB.181
1242 Zeebe, R. E., & Wolf-Gladrow, D. A. (2001). *CO_2 in seawater: equilibrium, kinetics,*
1243 *isotopes*. *Elsevier Oceanography Series*.
1244 Zhou, Y., Martin, P., & Müller, M. (2019). Composition and cycling of dissolved organic
1245 matter from tropical peatlands of coastal Sarawak, Borneo, revealed by fluorescence
1246 spectroscopy and parallel factor analysis. *Biogeosciences*, *16*(13), 2733–2749.
1247 https://doi.org/10.5194/bg-16-2733-2019
1248 Zhu, Z.-Y., Oakes, J., Eyre, B., Hao, Y., Sia, E. S. A., Jiang, S., et al. (2020). The
1249 nonconservative distribution pattern of organic matter in the Rajang, a tropical river with
1250 peatland in its estuary. *Biogeosciences*, *17*(9), 2473–2485. https://doi.org/10.5194/bg-
1251 17-2473-2020
1252 Zigah, P. K., McNichol, A. P., Xu, L., Johnson, C., Santinelli, C., Karl, D. M., & Repeta, D.
1253 J. (2017). Allochthonous sources and dynamic cycling of ocean dissolved organic

1254 carbon revealed by carbon isotopes. *Geophysical Research Letters*, *44*(5), 2407–2415.

1255 https://doi.org/10.1002/2016GL071348

1256